CrossMark
click for updates

Leveraging valuable synergies by combining alloying and conversion for lithium-ion anodes†

Dominic Bresser,[a] Stefano Passerini*[bc] and Bruno Scrosati*[bde]

The essential need for new lithium-ion battery materials providing higher energy and power densities has triggered an exceptional increase in scientific and industrial research efforts in recent years. Regarding the anode side, the two major research directions to achieve improved energy densities have, so far, focused on materials which can host lithium either by alloying or by a conversion mechanism. Very recently, however, a new class of potential next generation anodes is gaining continuously increasing attention: conversion/alloying materials. Herein, we provide for the first time a comprehensive review on this new materials' class. Initially, we discuss the two possible approaches to realize a combined conversion and alloying mechanism in a single compound, starting either from pure conversion or pure alloying materials. Based on this overview we subsequently highlight the fundamental insights and their potential advantages, which shall provide scientists with some general considerations and principles for the development of new, further enhanced conversion/alloying materials.

Broader context
Lithium-ion batteries, commercialized for the first time by SONY Corp. in 1991, have marked a breakthrough in the field of electrochemical energy storage, providing energy and power densities 2 to 10 times greater than any other battery chemistry. For this reason, they are already the technology of choice for portable electronics and also for large-scale applications like electric vehicles and stationary energy storage. Particularly for the latter ones, however, further improvement is needed and after substantial enhancement by engineering-driven advances, including, for instance, the electrode and cell design, the next great leap forward will require the implementation of new chemistries, replacing the state-of-the-art active materials, *i.e.*, lithium transition metal oxides or lithium iron phosphate and graphite on the cathode and anode side, respectively. Alternative cathode materials with great potential are certainly sulfur or oxygen, while research activities targeting the development of alternative anode materials focused initially on metallic lithium, alloying, and conversion compounds. Recently, however, a new class of alternative anodes is attracting continuously increasing attention: conversion/alloying materials, which combine these two reaction mechanisms in one single compound.

1. Introduction and outline

Lithium-ion batteries, LIBs, are at present the power sources of choice for small- and medium-scale applications like portable electronic devices such as smartphones, laptops, camcorders, and increasingly also electric bikes and scooters (Fig. 1).[1–5] The main driving force for developing LIBs providing further enhanced energy and power densities, however, is certainly the need for highly efficient, long-term reliable, lightweight, and competitive energy storage systems for expanding the electrification of modern society's public and private transportation sector based on renewable energy sources (Fig. 1).[5–9]

While on the cathode side environmentally benign and abundant materials like sulphur and oxygen hold great promise for realizing next generation batteries with energy densities approaching those of gasoline-powered vehicles,[10–15] the utilization of such high energy cathodes consequently calls also for high energy anode materials, as schematically illustrated in Fig. 2. The ideal anode candidate would be, without a doubt, metallic lithium (Fig. 2a). Nonetheless, despite substantial improvements in overcoming interfacial and cycling efficiency issues by using, for instance, ionic liquid-,[16,17] polymer-based,[18,19] or solid[20,21] electrolytes or protecting the lithium metal surface with carbon,[22] the severe safety issues related to dendrite growth and its high reactivity still remain to be completely solved.[23]

[a] CEA-Grenoble, DRF/INAC/SPrAM/PCI, 17 Rue des Martyrs, 38054 Grenoble, France. E-mail: dominic.bresser@kit.edu
[b] Helmholtz-Institute Ulm (HIU), Electrochemistry of the Battery, Helmholtzstrasse 11, 89081 Ulm, Germany. E-mail: bruno.scrosati@gmail.com
[c] Karlsruher Institute of Technology (KIT), PO Box 3640, 76021 Eggenstein-Leopoldshafen, Germany. E-mail: stefano.passerini@kit.edu
[d] Elettrochimica ed Energia (EeE), 00199 Rome, Italy
[e] Italian Institute of Technology (IIT), Via Morego 30, 16163 Genova, Italy
† Electronic supplementary information (ESI) available. See DOI: 10.1039/c6ee02346k

3348 | *Energy Environ. Sci.*, 2016, **9**, 3348–3367

This journal is © The Royal Society of Chemistry 2016

For this reason, several groups started to investigate the combination of sulphur- or oxygen-based cathodes with alternative anode materials like silicon[24–27] or tin,[28,29] which can reversibly alloy with lithium upon discharge (see Fig. 2b for the case of tin). Such alloying materials, comprehensively reviewed very recently by Obrovac and Chevrier,[30] generally offer high specific capacities (e.g., 993 mA h g^{-1} in case of tin and up to 3578 mA h g^{-1} in case of silicon) and commonly operate at reasonable low potentials, rendering them generally as very attractive alternatives for the state-of-the-art lithium-ion anode graphite (372 mA h g^{-1}).[30–34]

Fig. 1 Schematic drawing of the general working principle (on the right) of lithium-ion batteries, with lithium cations shuttling from one electrode to the other accompanied by a unidirectional electron transfer along an outer circuit, and their current and foreseen applications (on the left), ranging from portable electronic devices to electrified transportation, including electric scooters and vehicles, as well as stationary energy storage for renewables.
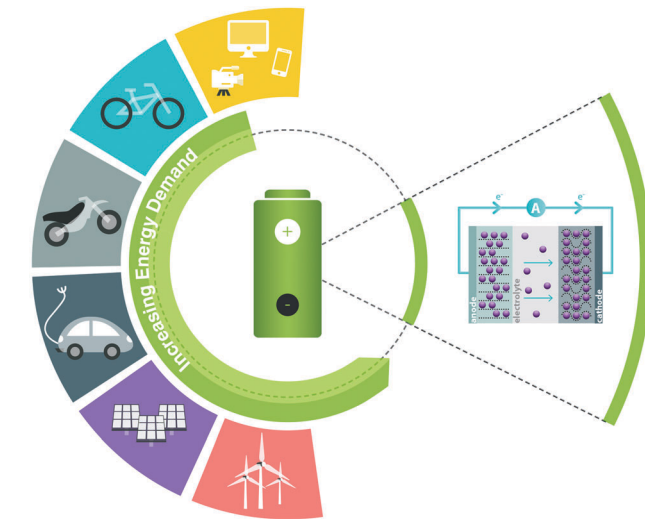
Dominic Bresser

Dominic Bresser is currently holding a postdoctoral position and Enhanced Eurotalents Fellowship at the Commissariat à l'Energie Atomique et aux Energies Alternatives (CEA) in Grenoble, France in the group of Dr Sandrine Lyonnard, where he is studying new electrolyte systems, including nanostructured single-ion conductors and polymerized ionic liquids. Prior to this, he carried out his PhD in the group of Professor Stefano Passerini at the University of Muenster (Germany) and at the Helmholtz Institute Ulm (HIU; affiliated with the Karlsruher Institute of Technology, KIT), investigating nanostructured active materials for lithium-based batteries. He is Co-Author of more than 40 scientific publications (h-index of 19), including two book chapters, and several international patent applications.

But their widespread implementation in practical lithium-ion cells is hampered by the extensive volume changes upon (de-)lithiation of up to about 300%.[30–34] In an attempt to circumvent this issue, it was proposed to utilize the corresponding oxides (e.g., SnO$_2$), thus benefitting from the initial irreversible formation of a lithium oxide (Li$_2$O) matrix, which buffers the occurring volume variations upon subsequent (de-)lithiation of the simultaneously formed metallic nanograins.[35–38]

Stefano Passerini

Stefano Passerini is Professor at the Karlsruhe Institute of Technology (KIT), Helmholtz Institute Ulm (HIU, Germany) since January 1, 2014. Formerly Professor at the University of Muenster (Germany), he co-founded the MEET battery research centre (Muenster, Germany). His research activities are focused on electrochemical energy storage in batteries and supercapacitors. He is co-author of more than 400 scientific papers (h-index of 58), a few book chapters and several international patents. In 2012, he has been awarded the Research Award of the Electrochemical Society Battery Division. Since 2015 he has been appointed as Editor-in-Chief of the Journal of Power Sources.

Bruno Scrosati

Bruno Scrosati, formerly Full Professor at the University of Rome, is presently affiliated with the Italian Institute of Technology (IIT, Italy) and visiting professor at the Helmholtz Institute Ulm (HIU, Germany). He received the Doctor in Science honoris causa from the University of St. Andrews (UK), the Chalmers University (Sweden) and the University of Ulm (Germany). He received the Research Award from the Battery Division of the Electrochemical Society (ECS), the XVI Edition of the Italgas Prize and the Vittorio de Nora award of the ECS. He has been President of the Italian Chemical Society and the ECS. He was European Editor of the Journal of Power Sources and is presently a member of Editorial Boards of various international journals. Professor Scrosati is the author of more than 550 scientific publications (h-index of 74), various books and book chapters, and 18 patents.
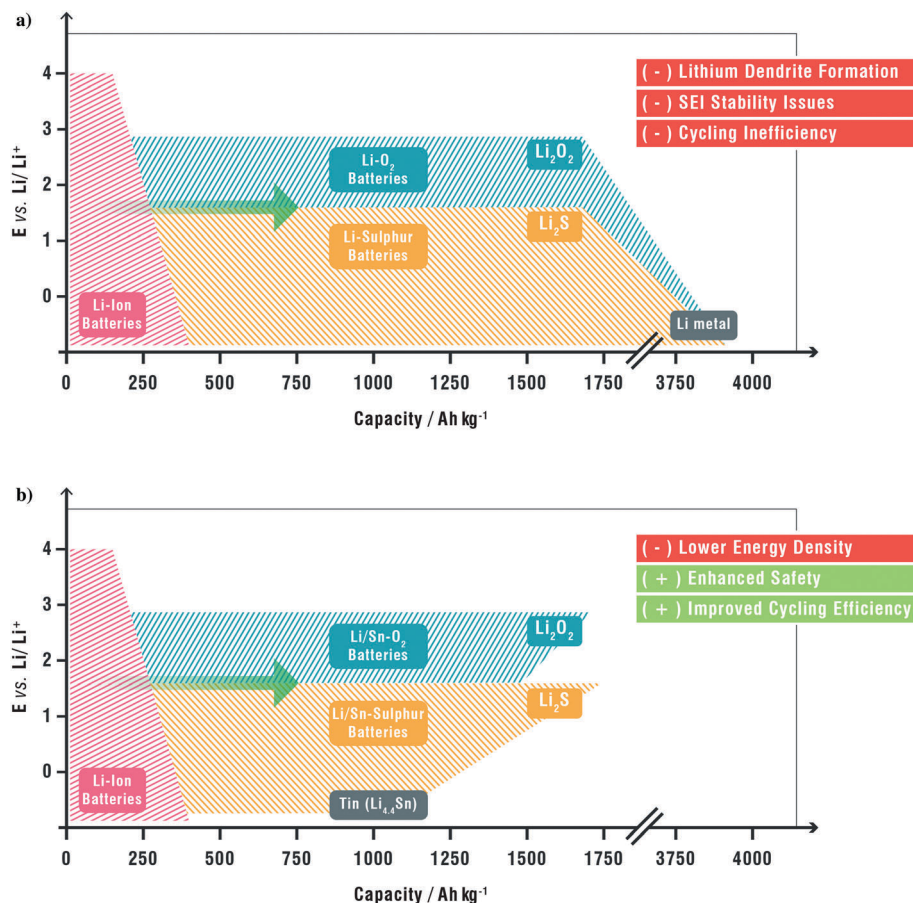
Fig. 2 Schematic graphic, depicting the shift from intercalation-based lithium-ion chemistry (green; graphite anode) to high-capacity next generation lithium-based batteries using oxygen (blue) or sulphur (yellow) as cathode materials and metallic lithium (a) or tin (b) a anode materials.

The reversible lithium storage mechanism occurring for the second major class of alternative high capacity anodes, the so-called conversion materials,[34,39–44] can, in fact, be considered, as exactly the opposite. In case of the most investigated group of such compounds – transition metal oxides (TMOs; with TM = e.g., Co, Fe, Ni, or Cu) – initially the same reaction occurs, i.e., the reduction of the TMO, forming metallic TM nanograins embedded in an amorphous matrix of lithium oxide.[39] Nevertheless, in this case the metallic nanoparticles remain electrochemically inactive and lithium oxide is formed reversibly. Such extensive bond cleavage and re-forming, however, results in a rather wide operational potential range and a large voltage hysteresis between charge and discharge, i.e., a relatively low energy storage efficiency.[34,40,41,45] The reaction mechanisms for these classic types of lithium ion storage (including intercalation for graphite) are schematically illustrated in Fig. S1 (ESI†).

In this article, we review for the first time the latest approach for developing high energy lithium-ion anode materials, targeting the beneficial combination of these two lithium storage mechanisms in a single compound, which we will hereinafter refer to as conversion/alloying materials, CAMs. Initially, we briefly survey pure conversion-type compounds with a particular focus on recently reported fundamental insights into the reaction mechanism. Based on this survey, we then present an overview on the first alternative to realize CAMs, i.e., the partial substitution of the electrochemically inactive TM in conversion-type compounds by elements which can further alloy with lithium as, for example, the case for $ZnTM_2O_4$ (with TM = Fe, Co, Mn). As a result, these materials provide significantly increased capacities compared to the pure conversion-type ones. In a next step, we introduce the second alternative to further increase the energy density of conversion/alloying materials by reversing this concept, i.e., starting from an alloying compound and enabling the reversible conversion, as realized, for instance, in TM-doped zinc or tin oxide.[46–50] This approach, indeed, follows the fundamental insight that the key to enable the reversibility of conversion reactions is the formation of an electronically conductive network of TM nanograins.[51–53] In combination with recent findings that some elements like Ge,[54] Sn,[55] or Zn[56] do not only form alloys but moreover potentially enable the reversible formation of Li_2O, an almost unlimited variation of new LIB anodes, offering tailored specific capacities and operational potentials, appears conceivable. Following these considerations, we finally discuss the potential advantages of CAMs compared to pure conversion and alloying materials and provide some general principles for the design of new members of the conversion/alloying class, which will ideally inspire scientists to develop further enhanced anodes for next generation lithium-based batteries.

2. Lithium storage by conversion

In 2000, Tarascon and co-workers reported for the first time the reversible electrochemical lithiation of transition metal (TM) oxides (TM = Co, Ni, Fe, Cu),[39] which was up to then considered to be irreversible.[57] These transition metal oxides host lithium by the following general displacement reaction mechanism, as later on confirmed *inter alia* also by *ex situ* X-ray photoelectron spectroscopy (XPS)[58] or *in situ* transmission electron microscopy (TEM):[59]

$$TM_xO_y + 2yLi^+ + 2ye^- \leftrightarrow xTM^0 + yLi_2O \quad (1)$$
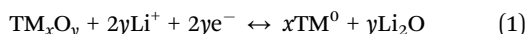
Due to their highly promising specific and, in particular, volumetric capacities – frequently up to two to six times higher than that of the state-of-the-art graphite anode (depending on the molar mass and oxidation state of the TM as well as the density of the oxide) – tremendous research efforts were undertaken since then to improve the understanding of this reaction mechanism and enhance the electrochemical properties of the conversion-type anodes. Moreover, it was found that such reversible displacement-type reactions occur likewise for a variety of other first-, second-, and third-row transition-metal-based oxides, including Mn,[60] Cr,[61] Mo,[62] Ru,[63] or W,[64] as well as the corresponding transition metal sulfides,[65] nitrides,[66] fluorides,[67] phosphides,[68] hydrides,[69] or carbonates.[70–72] All these compounds are commonly referred to nowadays as 'conversion materials' and an extensive review on this new materials' class was presented in 2010 by prolific and experienced researchers in this field.[41]

Herein, we will thus focus in particular on those studies reported after 2010 providing an enhanced understanding of the reaction mechanism, mainly carried out on transition metal oxides and fluorides. We may briefly note at this point that transition metal fluorides are considered as alternative high energy LIB cathodes rather than anodes due their relatively higher lithium reaction potential (>2 V), originating from the pronounced ionic character of the TM–F bond.[41] Nevertheless, it is commonly agreed on that the insights obtained for fluorides are applicable also for conversion materials in general. As a matter of fact, it was shown for both transition metal oxides[59,73] and fluorides,[51,74] that upon lithiation, *i.e.*, reduction, an interconnected, percolating network of metallic nanograins, having a size of about 1–3 nm, is formed. This metallic nano-network apparently serves as electron conduction pathway throughout the initial primary particle, thus ensuring the local availability of electrons for the reversible formation of the surrounding quasi-amorphous/nano-crystalline lithium oxide/fluoride. Consequently, the diffusivity of the transition metal cations is of great importance, as it determines the size of these metallic nanograins and, as a result, the realization of a continuous electron-conducting network.[51] This consideration was confirmed by comparing the lithiation of iron and copper fluoride – the latter, indeed, revealing significantly larger, isolated metallic nanograins (5–12 nm), due to the higher mobility of copper cations, and a lack of reversibility for the LiF formation.[51] Detailed TEM investigations of iron fluoride[52] and nickel oxide[53] nanoparticles

revealed, furthermore, comprehensive insights into the lithiation mechanism itself. While the mobility of lithium ions is very fast at the particle surface[52] and/or along the interface of initially already present as well as upon lithiation formed nano-domains,[53] its penetration into the bulk particle is relatively much slower,[52] suggesting that the conversion reaction takes place layer-by-layer,[52] preferably at the aforementioned interfaces,[75] which may result in a heterogeneous reaction front in larger particles.[53] Accordingly, the nano-crystalline (2–7 nm)[53] nature of the once lithiated particles,[39,59,74,76,77] indicated also by the subsequently sloped potential profile,[78] appears highly beneficial with respect to high-power application for such materials. In fact, even though the initial penetration into the bulk may be relatively slow, a particle with a size of about 10 nm can be fully lithiated within a few minutes, indicating that (dis-)charge rates of up to 20 C may be applied without substantial capacity loss,[52] which is in good agreement with earlier findings by Tarascon and co-workers for iron oxide nanoparticles grown directly on a nanostructured copper current collector.[45] These findings, however, challenge the initial suggestion[39,79] that the greatest issue of conversion-type materials towards their practical use in lithium-ion batteries, namely, the extensive voltage hysteresis between charge and discharge, resulting in a relatively low energy storage efficiency and internal heat evolution, thus, adding also a safety issue, originates from simple kinetics, related to the substantial structural rearrangement upon (de-)lithiation and the insulating nature of most conversion-type materials.[80,81] Indeed, neither cycling conversion-type electrodes at elevated temperature (*i.e.*, 100 °C),[82] nor the smart design of advanced nanostructures,[45,83] the incorporation of highly conductive carbonaceous nanomaterials,[84,85] the introduction of metallic dopants,[86] or the partial replacement of one transition metal by another to enhance the electronic conductivity[87] resulted in a significant decrease of the voltage hysteresis; though certainly enhancing the electrochemical performance in terms of cycling stability and rate capability.[88] Instead, based on density functional theory (DFT) calculations for FeF$_3$, Ceder and co-workers proposed that this voltage hysteresis may be related to different reaction paths for the lithiation and delithiation process, originating from the relatively higher mobility of lithium compared to iron ions, thus being intrinsic to the specific material and to its structure.[89]

The extensive study of nano-sized conversion electrodes, however, has emphasized another great challenge for the implementation of conversion-type materials in practical LIBs: the catalytically activated,[90,91] continuous electrolyte decomposition, augmented by the increased surface area and detrimentally affecting their cycling stability.[39,77] As this electrolyte decomposition appears to be partially reversible, it can be easily tracked by a capacity increase at low potentials upon lithiation (*ca.* <0.8 V) and high potentials upon delithiation (*ca.* >2.0 V).[92–94] This partial reversibility was initially assigned to the dissolution of organic, *i.e.*, oligomeric or polymeric $(CH_2–CH_2O)_n$-like electrolyte decomposition products.[58,95] A rather recent combined *ex situ* XPS and atomic force microscopy (AFM) study on CuO thin films, on the contrary, indicates that the partial reversibility may be ascribed to the dissolution of (large) Li_2CO_3 particles,

This journal is © The Royal Society of Chemistry 2016

Energy Environ. Sci., 2016, **9**, 3348–3367 | **3351**

which are formed at the electrode surface upon lithiation and are dissolved when the electrode is delithiated.[96] Considering the above mentioned reversible conversion reaction of transition metal carbonates,[70,71] and particularly of Li_2CO_3 in presence of the freshly formed transition metal nanograins,[72] this explanation appears conceivable.

This brief and certainly not exhaustive summary of recent findings on conversion-type materials illustrates that the most challenging issues towards their implementation in commercial cells still remain to be solved. But there has been also substantial progress. For instance, the issue of continuous electrolyte decomposition may be very well addressed by using internally nanostructured materials, i.e., relatively larger particles built up of nanodomains, thus providing an extensive network of interfaces for fast lithium transfer.[97] Another approach may be the passivation of the particle surface with protective coatings as, for instance, carbon[77,98] – an already very well established procedure for lithium-ion electrode materials – resulting in a stabilized solid electrolyte interphase (SEI) and preventing an intimate contact between the conversion material particles and the electrolyte. Also, as reported by Oumellal et al.,[69] the voltage hysteresis appears to be highly dependent on the nature of the anion, decreasing along the following trend: fluorides > oxides > sulfides > nitrides > phosphides > hydrides. Interestingly, this trend is in rather good agreement with Pearson's concept of hard and soft acids and bases,[99,100] giving hope that further progress can be achieved to enhance the energy storage efficiency and reduce the (de-)lithiation potential range of conversion-type electrodes.

And not least, several recent lithium-ion full-cell studies employing conversion anodes have shown very promising performance, as nicely reviewed by Aravindan et al.[101] Especially, a composite of porous carbon and Fe_3O_4 combined with a $Li[Ni_{0.59}Co_{0.16}Mn_{0.25}]O_2$-based cathode[102] as well as a composite of perforated graphene and Fe_3O_4 combined with a $LiMn_2O_4$[103] cathode revealed exceptional cycling stabilities with a capacity retention of about 64% after 1000 cycles and around 66% after 10 000 cycles, respectively. It should be noted, though, that this outstanding performance was achieved by pre-lithiating both anode composites in order to bypass the initial charge loss, which would result in a significant decrease in energy density due to the need of an oversized cathode.[104] To be noticed, however, that a high initial charge loss is not only an issue related to conversion-type materials and recently emerged strategies, like the addition of sacrificial lithium salts to the cathode electrode composite,[105] the utilization of stabilized lithium powders,[106] or the implementation of an internal lithium source[107] hold the great promise that it may be overcome soon.

3. From conversion to conversion/alloying

3.1 The general concept

According to an estimation of Badway et al.[104] conversion-type anodes may compete energy-density-wise with graphite only if

they provide specific capacities in the range of 1000 mA h g^{-1} and react with lithium at voltages lower than 0.6 V when assuming an initial capacity loss of around 25%. In fact, from a safety point of view it would be highly desirable to replace graphite by alternative anode materials, hosting lithium at relatively higher voltage. Apart from the other challenges, which were discussed in the previous section, most conversion-type materials, however, provide specific capacities lower than 1000 mA h g^{-1} at average voltages higher than 0.6 V. Co_3O_4 or Fe_3O_4, for instance, offer theoretical specific capacities of about 890 and 926 mA h g^{-1} at average delithiation voltages of around 2.0 V[77] and 1.8 V,[108] respectively. It is thus, indispensible to further increase the capacity and decrease the operational potential range, if such materials shall become commercial reality.

One approach, to address these two issues is the partial replacement of the electrochemically inactive transition metal by an element which can reversibly form an alloy with lithium. In addition to the thus increased number of lithium ions hosted per formula unit, such alloying materials commonly react with lithium at significantly lower voltages,[30,31,34] potentially resulting in a decreased overall reaction voltage. As these substances accordingly combine both lithium storage mechanisms in one single compound, we will refer to them herein in the following as 'conversion/alloying materials', CAMs. In this case, the initially formed Li_2O matrix, supported by the electron conducting TM^0 nano-network, has also a buffering effect for the alloying reaction, thus, beneficially combining the advantages of the two reaction mechanisms (Fig. 3). While showing some similarities with the concept of intermetallic alloying compounds,[109,110] the combination of conversion and alloying in a single compound provides the additional benefits of a very fine distribution of the alloying element (initially on the atomic scale) and the substantially lower volume expansion (40–100%)[52,59,76] and particle morphology evolution[53,111–113] of conversion materials. Nonetheless, as both mechanisms are characterized by significant volume variations and structural rearrangement, the final lithium storage properties and the reversibility of the (de-)lithiation reaction remain highly dependent on the particle and electrode architecture. It is thus not surprising that the advent of nanotechnology and the continuously increasing interest in such
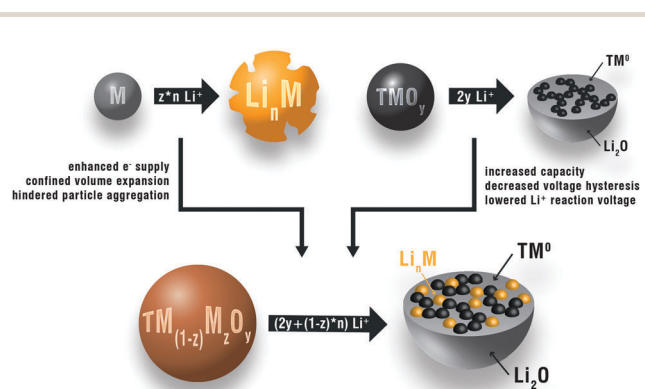

Fig. 3 Illustrative summary of the beneficial combination of conversion- and alloying-type lithium storage in conversion/alloying materials (CAMs).

materials has recently led to great improvements regarding their electrochemical performance.

3.2 Introduction of zinc in transition metal oxides

The most investigated family of CAMs are spinel-structured transition metal oxides, for which one transition metal cation is replaced by divalent zinc, $ZnTM_2O_4$ (with TM = Fe, Co, or Mn), as zinc can itself reversibly form an alloy with lithium,[114] thereby increasing the total number of lithium ions hosted per unit formula from eight (as for, *e.g.*, Co_3O_4, Mn_3O_4, or Fe_3O_4) to nine:

$$ZnTM_2O_4 + 8Li^+ + 8e^- \rightarrow 2TM^0 + 4Li_2O + Zn^0 \quad (2)$$

$$Zn^0 + Li^+ + e^- \rightarrow LiZn \quad (3)$$
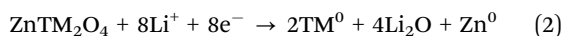
And among the three 'classic' representatives of this concept – $ZnFe_2O_4$ (ZFO), $ZnCo_2O_4$ (ZCO), $ZnMn_2O_4$ (ZMO) – ZFO is at present the most and, in fact, also the first studied compound. In 1986, Chen *et al.*[115] investigated the possible application of ZFO as active material for lithium-based batteries, assuming that lithium ions may be reversibly inserted into the spinel framework. However, the chemical lithiation was limited to a maximum uptake of 0.5 lithium ions per formula unit of ZFO and did not appear reversible. The achievement of substantially higher and, in particular, reversible lithium storage was then reported in 2004 by NuLi *et al.*,[116] studying the electrochemical lithiation of nanocrystalline ZFO thin films. They observed reversible specific capacities of around 560 mA h g^{-1}, *i.e.*, about half of the theoretical value of 1000.5 mA h g^{-1} (see Table 1). Subsequent studies of Sharma *et al.*[117] on submicron-sized particles in 2008 and Guo *et al.*[118] on hollow spherical particles in 2010 revealed further increased capacities up to about 900 mA h g^{-1}, *i.e.*, approaching the theoretical maximum value. In addition, Guo *et al.*[118] performed an *ex situ* selected area electron diffraction (SAED) characterization and confirmed the

earlier proposed[117] formation of Li–Zn and metallic iron in the fully lithiated state and ZnO and Fe_2O_3 in the fully delithiated state, which was later on affirmed *inter alia* by Xing *et al.*[119]

$$2Fe^0 + 4Li_2O + LiZn \leftrightarrow ZnO + Fe_2O_3 + 9Li^+ + 9e^- \quad (4)$$
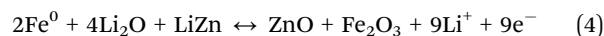
Similarly, it was reported that $ZnCo_2O_4$ (ZCO), firstly reported as lithium-ion anode in 2004 as well,[120] and $ZnMn_2O_4$ (ZMO), reported for the first time in 2008,[121] reversibly form zinc oxide and cobalt oxide (4), respectively, manganese oxide (5) after the first lithiation. Nevertheless, in both cases, the detailed reaction mechanism is not fully clarified, yet. Some studies detected only Co_3O_4[122,123]/Mn_3O_4[124] in the delithiated state, while others identified a mixture of the respective monoxide and the spinel-structured oxide, *i.e.*, CoO/Co_3O_4[125] and MnO/Mn_3O_4.[126] It is apparently challenging to stoichiometrically balance the following two eqn (5) and (6) without assuming either an additional oxygen source or oxygen-deficient metal oxide phases. Since this question remains to be properly addressed, we may simply refer herein to an oxide phase with an undetermined TM : O ratio, including also the possible presence of different transition metal oxide phases:

$$2Co^0 + 4Li_2O + LiZn \leftrightarrow ZnO + Co_xO_y + 9Li^+ + 9e^- \quad (5)$$

$$2Mn^0 + 4Li_2O + LiZn \leftrightarrow ZnO + Mn_xO_y + 9Li^+ + 9e^- \quad (6)$$
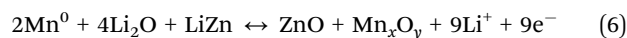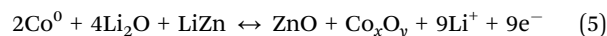
Accordingly, we may thus express the general reversible (de-)lithiation reaction for spinel-structured $ZnTM_2O_4$ as follows:

$$2TM^0 + 4Li_2O + LiZn \leftrightarrow ZnO + TM_xO_y + 9Li^+ + 9e^- \quad (7)$$
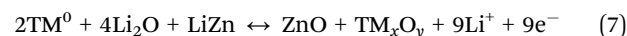
Apart from such fundamentally important studies, targeting an enhanced understanding of the detailed reaction mechanism, the majority of the published research activities focused on the improvement of the electrochemical performance when used as lithium-ion anode. For this purpose, basically four approaches

Table 1 Recapitulatory overview of the herein presented conversion/alloying materials and their main electrochemical properties as lithium-ion anodes

	Theoretical Li uptake per formula unit [#]	Theoretical specific capacity/mA h g^{-1}	Contribution of the alloying reaction [%]	Average delithiation voltage(s)/V *vs.* Li/Li$^+$
$ZnFe_2O_4$	9	1000.5	11.1	1.5^a/1.75
$ZnCo_2O_4$		975.5		1.65^a/2.1
$ZnMn_2O_4$		1008.1		1.2/1.6^a
Co_2SnO_4	12.4	1105.7	35.5	0.55^b/2.0
Mn_2SnO_4		1135.9		0.55^b/1.25
Ni_2SnO_4		1107.5		0.56^b/2.1
$CoSnO_3$	10.4	1235.3	42.3	0.6^b/2.1
$NiSnO_3$		1236.6		0.55^b/2.2
$Zn_{0.9}Fe_{0.1}O$	2.9	966.1	31.0	1.3^c
$Zn_{0.9}Co_{0.1}O$		962.4		1.4^c
$Sn_{0.9}Fe_{0.1}O_2$	7.96	1477.2	49.7	0.5^b/1.5
Co_2SiO_4	4	510.6	0	$\sim$2.0
Fe_2SiO_4		526.1		$\sim$2.0
Mn_2SiO_4		530.8		$\sim$1.4

^{a} According to Teh *et al.*[249] the delithiation voltages of 1.5–1.65 V are ascribed to the re-oxidation of Zn^0. ^{b} Assigned to the dealloying of initially formed metallic tin. ^{c} These values were determined as the delithiation voltage at which half of the hosted lithium was released. Generally, it should be noted that the here given values are dependent on the applied current or sweep rate as well as the internal resistance of the cell and may thus be considered more as a coarse guideline. Also, please note that the TM_2SnO_4- and $TMSnO_3$-type stannates commonly show a rather sloped potential profile between the two given values, which may be characterized by additional features related to the re-oxidation of tin, though apparent frequently only in the corresponding CV curves.

have been (partially simultaneously) followed for this materials' class (Fig. 4; selected examples are also presented in Table 2):

(1) Synthesis and design of (meso-)porous micro-sized secondary particles, built up out of very fine nanocrystals, for which the porous structure may buffer the occurring volume variations while the nanosize of the primary particles allows for short lithium and electron transport pathways[123,125,127–130] (Fig. 4a).

This approach has particularly provided an excellent impression of the steadily improving ability of scientists to develop smartly designed new material architectures using advanced synthesis techniques, including the realization of (hollow) submicro- and micro-spheres,[131–134] "yolk–shell" or "ball-in-ball" structures,[135–137] (sub-)micro-cubes,[134,138] and (hollow) porous micro-polyhedra.[139–141] And apart from the frequently rather complex synthesis procedures, these compounds commonly show enhanced specific capacities, cycling stability, and rate capability. Mesoporous ZCO twin microspheres,[134] for instance, revealed an impressive high rate performance, offering specific capacities of 920 and 790 mA h g^{-1} for applied currents of 5.0 and 10.0 A g^{-1}, respectively, and a capacity retention of 550 mA h g^{-1} after 2000 cycles at 5.0 A g^{-1}. Similarly, superior lithium storage capability was reported for porous (core–shell)[137] ZMO microspheres, presenting a stable capacity of 800 mA h g^{-1} for more than 300 cycles[128] and capacities of about 610, 530, and 460 mA h g^{-1} for specific currents of 1.0, 2.0, and 4.0 A g^{-1}, respectively.[137] When investigating the impact of the particle morphology and shape, it was moreover found that octahedrally-shaped ZFO particles appear advantageous concerning their electrochemical properties as anodes,[119,142] which Zhong et al.[142] attributed to the relatively larger fraction of {111} surface planes, though this is not completely understood, yet. Despite these great advantages of mesoporous, highly nanocrystalline structures, however, their intrinsically large surface area also leads to relatively lower coulombic efficiencies due to the aforementioned high reactivity of transition metals towards state-of-the-art organic electrolytes.[90,91]

(2) Introduction of carbonaceous particles and nanostructures to enhance the electronic conductivity within the electrode and to avoid the loose of contact upon continuous (de-)lithiation by forming strong interactions between the carbonaceous hetero-structures and the active material nanoparticles (Fig. 4b).

The incorporation of carbonaceous particles and nanostructures as, for instance, graphite flakes,[143] carbon nanotubes (CNTs),[144] 3-dimensional (3D) porous carbons,[145,146] or graphene[147–151] mainly targets the realization of percolating electron conducting networks within the final electrode composition and enables the utilization of very fine nanoparticles (frequently <20 nm) without facing severe particle agglomeration upon electrode preparation and/or cycling. Accordingly, such active material/carbon composites commonly show improved cycling stability and rate capability. Very impressive results were inter alia reported by Xiong et al.[149] for a chemically integrated ZMO/graphene composite, achieving an outstanding cycling stability of 1500 cycles with a specific capacity of more than 600 mA h g^{-1} at 2.0 A g^{-1} and still 570 mA h g^{-1} for a further increased specific current of 3.2 A g^{-1}. Nevertheless, depending on the amount of carbonaceous additives, this approach may lead to decreased gravimetric capacities and, more importantly, the issue of the insufficiently stable ZnTM$_2$O$_4$/electrolyte interface remains to be solved.

(3) Application of polymeric or carbonaceous coatings to buffer occurring volume changes, enhance the electronic conductivity, and passivate the highly reactive ZnTM$_2$O$_4$ (nano-)particle surface in order to stabilize the electrode/electrolyte interface and prevent continuous electrolyte decomposition (Fig. 4c).
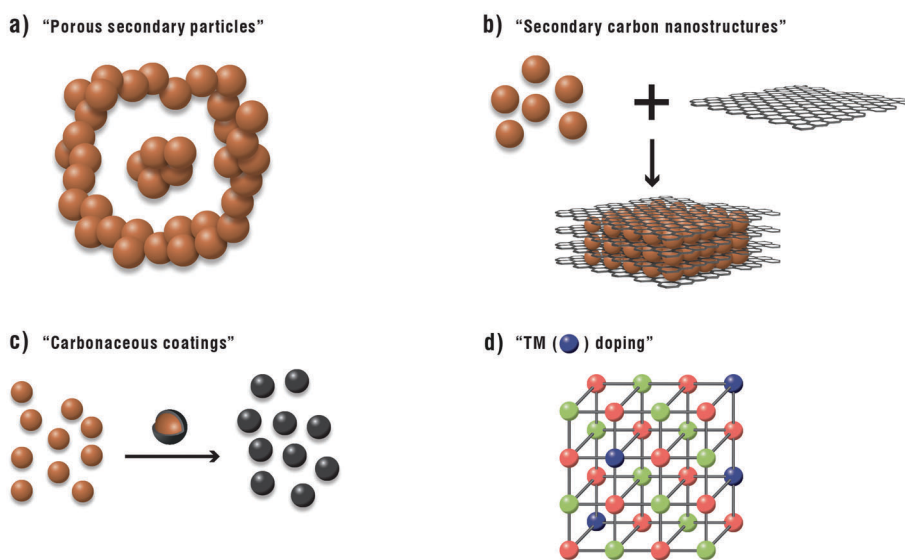
Fig. 4 Schematic illustration of the basic four approaches to enhance the electrochemical performance of CAMs: (a) porous micro-sized secondary particles (e.g., yolk–shell structures), (b) introduction of carbonaceous secondary nanostructures (e.g., graphene nanocomposites), (c) carbonaceous coatings, and (d) transition metal (TM) doping (anions in red, cations in green; for clarity reasons only one color is used for the initially present cations).

3354 | Energy Environ. Sci., 2016, 9, 3348–3367

This journal is © The Royal Society of Chemistry 2016

Table 2 Overview of reported electrochemical performances for selected CAMs in lithium-ion half-cell configuration

Approach(es)	Example	Specific capacity/ mA h g^{-1}	Specific current/ A g^{-1}	Long-term cycling capability	Electrode composition [active material : conductive carbon : binder]/wt%	Ref.
(1)	Hollow ZnCo$_2$O$_4$ dodecahedra	886 692 575	4.5 7.2 9.0	990 mA h g^{-1} after 50 cycles at 0.1 A g^{-1}	80:10:10	141
	Mesoporous ZnCo$_2$O$_4$ twin microspheres	1005 920 790	2.0 5.0 10.0	550 mA h g^{-1} after 2000 cycles at 5.0 A g^{-1}	70:20:10	134
	Porous ZnMn$_2$O$_4$ microspheres	896 654 496	0.2 0.5 1.0	800 mA h g^{-1} after 300 cycles at 0.5 A g^{-1}	75:15:10	128
(1) & (2)	Mesoporous ZnFe$_2$O$_4$ submicro-spheres/graphene composite	940 820 650	0.5 1.0 2.0	970/770 mA h g^{-1} after 200/500 cycles at 0.5/1.0 A g^{-1}	70*:20:10 (*incl. 22% graphene)	148
(2)	ZnMn$_2$O$_4$/graphene nanosheets	806 568	0.2 3.2	650 mA h g^{-1} after 1500 cycles at 2.0 A g^{-1}	90*:—:10 (*incl. 22.5% graphene)	149
	Co$_2$SnO$_4$/graphene nanocomposite	1103 910 797 710	0.1 0.25 0.5 1.0	1046 mA h g^{-1} after 100 cycles at 0.1 A g^{-1}	50*:30:20 (*incl. 9% graphene)	180
	CoSnO$_3$/graphene nanocomposite	957 829 706 539	0.1 0.2 0.4 0.8	724 mA h g^{-1} after 50 cycles at 0.05/0.2 A g^{-1} for discharge/charge	75*:10:15 (*incl. 19% graphene)	190
(1) & (3)	Porous, hollow ZnFe$_2$O$_4$/ZnO/C octahedra	934 887 842 762	1.0 2.0 5.0 10.0	988 mA h g^{-1} after 100 cycles at 2.0 A g^{-1}	70*:15:15 (*incl. 20% carbon & 22% ZnO)	139
	Porous Mn$_2$SnO$_4$/Sn/C cubes	971 775 550	0.5 1.0 2.0	908 mA h g^{-1} after 100 cycles at 0.5 A g^{-1}	80*:10:10 (*incl. 13% carbon)	185
(2) & (3)	Carbon-coated ZnFe$_2$O$_4$ nanoparticles/graphene composite	585 505 404	0.93 1.86 4.64	705 mA h g^{-1} after 180 cycles at 0.23 A g^{-1}	80*:10:10 (*incl. 38% carbon & graphene)	150
(3)	Carbon-coated ZnFe$_2$O$_4$ nanowires[153]/nanoparticles[154,155]	997[153] 862[153] 750[153] 310[154] 216[155]	0.1[153] 1.6[153] 3.2[153] 7.8[154] 20.0[155]	1091 mA h g^{-1} after 190 cycles at 0.1 A g^{-1}[155]	80*:10:10[153] (*incl. 2.5% carbon) 75*:20:5[154] (*incl. 13% carbon) 80*:10:10[155] (*incl. 14% carbon)	153–155
	Carbon-coated Zn$_{0.9}$Fe$_{0.1}$O nanoparticles	720 670 580 475 360	0.1 0.19 0.48 0.95 1.9	800 mA h g^{-1} after 30 cycles at 0.05 A g^{-1}	75*:20:5 (*incl. 18.5% carbon)	46
	Carbon-coated Sn$_{0.9}$Fe$_{0.1}$O$_2$ nanoparticles	1726/1360* (*incl. the carbon)	0.05	1519/1195* mA h g^{-1} after 10 cycles at 0.05 A g^{-1}	75*:20:5 (*incl. 21% carbon)	50
(4)	Mn-doped ZnFe$_2$O$_4$ nanoparticles	900 790	0.5 1.0	~100% capacity retention after 50 cycles at 0.1 A g^{-1}	50:30:20	164

This journal is © The Royal Society of Chemistry 2016

Energy Environ. Sci., 2016, 9, 3348–3367 | 3355

While the application of polymer particle coatings like polyaniline[132] or polypyrrole[152] showed some promising results and is of particular interest for lithium-ion polymer batteries, the best electrochemical performances following this approach were so far obtained for carbon-coated $ZnTM_2O_4$ nanostructures. Carbon-coated ZFO, for instance, revealed excellent high-rate capability, providing specific capacities of 750 mA h g^{-1} at 3.2 A g^{-1},[153] 525 mA h g^{-1} at 3.9 A g^{-1},[154] 400 mA h g^{-1} at 4.6 A g^{-1},[150] 310 mA h g^{-1} at 7.8 A g^{-1},[154] and still 216 mA h g^{-1} at a specific current as high as 20.0 A g^{-1},[155] which was assigned to the decreased charge transfer resistance, originating from the enhanced electronic conductivity.[156,157] The improved properties may, however, in part also be related to the substantially stabilized electrode/electrolyte interface[158–161] and inhibited ion dissolution,[155] as a direct contact between the $ZnTM_2O_4$ particles and the electrolyte is prevented. In fact, it is well known that carbonaceous anodes generally form very stable solid electrolyte interphases.[162] This is also true for carbon-coated ZFO, as very recently confirmed by *in situ* Raman spectroscopy[160] and *ex situ* X-ray absorption spectroscopy (XAS).[159,161] Another at least as important finding was reported by Kim *et al.*,[153] who observed that the voltage hysteresis, discussed in detail in Section 2, may be, indeed, substantially reduced for carbon-coated ZFO to about 0.5 V, if the kinetic contribution may be further reduced by designing advanced electrode architectures, *e.g.*, by combining carbonaceous coatings and graphene-based heterostructures.[150] As a matter of fact, these results render the application of carbonaceous coatings most promising for the development of advanced lithium-ion conversion/alloying-type anodes.

(4) Doping with transition metal cations, providing different valence states to increase the electronic conductivity of the CAM itself (Fig. 4d).

This approach has been studied only very rarely so far. In fact, the partial substitution of zinc by nickel resulted in an inferior capacity retention for nanocrystalline ZFO.[163] Contrarily, the incorporation of manganese[164] instead of zinc lead to enhanced specific capacities, cycling stability, and also rate capability, which the authors assigned to a reduced charge transfer resistance.[164] Apparently, however, further comprehensive studies will be required to investigate the potential beneficial impact of transition metal doping before any conclusion can be drawn.

3.3 $ZnTM_2O_4$ anodes in lithium-ion full-cells

Nonetheless, these approaches did not only show great promise in so-called half-cell studies, *i.e.*, using metallic lithium as counter electrode, thus providing an almost unlimited amount of lithium, but also in lab-scale lithium-ion battery prototypes. For instance, following the first two, Liu *et al.*[165] reported a very flexible 3D anode design by growing porous ZCO nanowires directly on a carbon cloth (Fig. 5a). By this, they ensured an excellent electronic wiring while also realizing sufficient space between the single nanowires to leave room for the occurring volume changes. This anode coupled with a conventional $LiCoO_2$-based cathode in an anode-limited full-cell assembly

revealed a capacity retention of 96% after 40 cycles (Fig. 5b), hence, presenting a great proof of concept that such anodes may be very well utilized in flexible lithium-ion cells. Extended long-term cycling was then reported by Xiong *et al.*[151] who combined a pre-lithiated ZMO/graphene composite (Fig. 5c) and 2D $LiFePO_4$ (LFP) nanosheets in a cathode-limited flexible full lithium-ion cell, which showed highly stable cycling at various (dis-)charge rates, providing about 90%, 74%, 57%, and 48% of the initial capacity at 0.075 A g^{-1} when elevating the applied current to 0.15, 0.3, 0.75 and 1.5 A g^{-1} (each for 100 cycles), *i.e.*, a power-performance superior to a standard graphite/LFP lithium-ion cell (Fig. 5d). Based on these results, the authors calculated a gravimetric energy of around 231 W h kg^{-1} and a specific power of 1.06 kW kg^{-1} for their full-cell at relatively lower and higher currents, respectively. A slightly lower energy (202 W h kg^{-1}), but substantially higher power (3.72 kW kg^{-1}) was reported finally by Varzi *et al.*[166] for carbon-coated, nanoparticulate ZFO anodes coupled with LFP/CNTs composites as cathodes. In addition to this outstanding high-power performance, the assembled lithium-ion full-cells revealed a capacity retention of 85% after 10 000 full charge/discharge cycles (Fig. 5e–g). Remarkably, the reaction voltage of the anode appeared highly dependent on the initial degree of lithium doping, *i.e.*, the buildup of an internal lithium reservoir in the anode, resulting in an increased full-cell output voltage by 0.43 V and a substantially lowered voltage hysteresis (Fig. 5h). While, in particular, the latter finding nicely emphasizes the impact of the alloying contribution at lower voltages on the achievable energy density and energy storage efficiency, these full-cell studies also show that $ZnTM_2O_4$-type CAM-anodes appear more suitable for high-power rather than high-energy applications. In fact, the specific energy of state-of-the-art lithium-ion batteries is about 200 W h kg^{-1} on the cell level (depending on the cell chemistry, electrode composition, packing density, *etc.*),[9,167,168] *i.e.*, higher than the values which may be expected for $ZnTM_2O_4$-comprising lithium-ion batteries. However, they largely exceed the specific energy values reported for lithium-ion capacitors, considered as a bridging technology between high-energy batteries and high-power capacitors, by about 60–100%, while providing a comparable specific power[169–171] and excellent reversibility of the lithium uptake and release.

3.4 General considerations regarding the transition metal

We may briefly note an important aspect at this point: Even though we reviewed ZFO, ZCO, and ZMO herein collectively, due to their very similar reaction mechanisms, resulting in the same materials' challenges and strategies to overcome these, they may not appear one as promising as the other regarding their application in practical lithium-ion batteries. First and rather obvious, ZFO and ZMO are certainly advantageous considering their cost, environmental impact, and biocompatibility, since they do not comprise high priced and toxic cobalt. Even more importantly, ZFO and ZMO provide slightly higher capacities due to the lower atomic mass of iron and manganese and substantially lower lithium reaction voltages (see Table 1 and Fig. 6), related to their relatively lower standard redox potentials.[172]
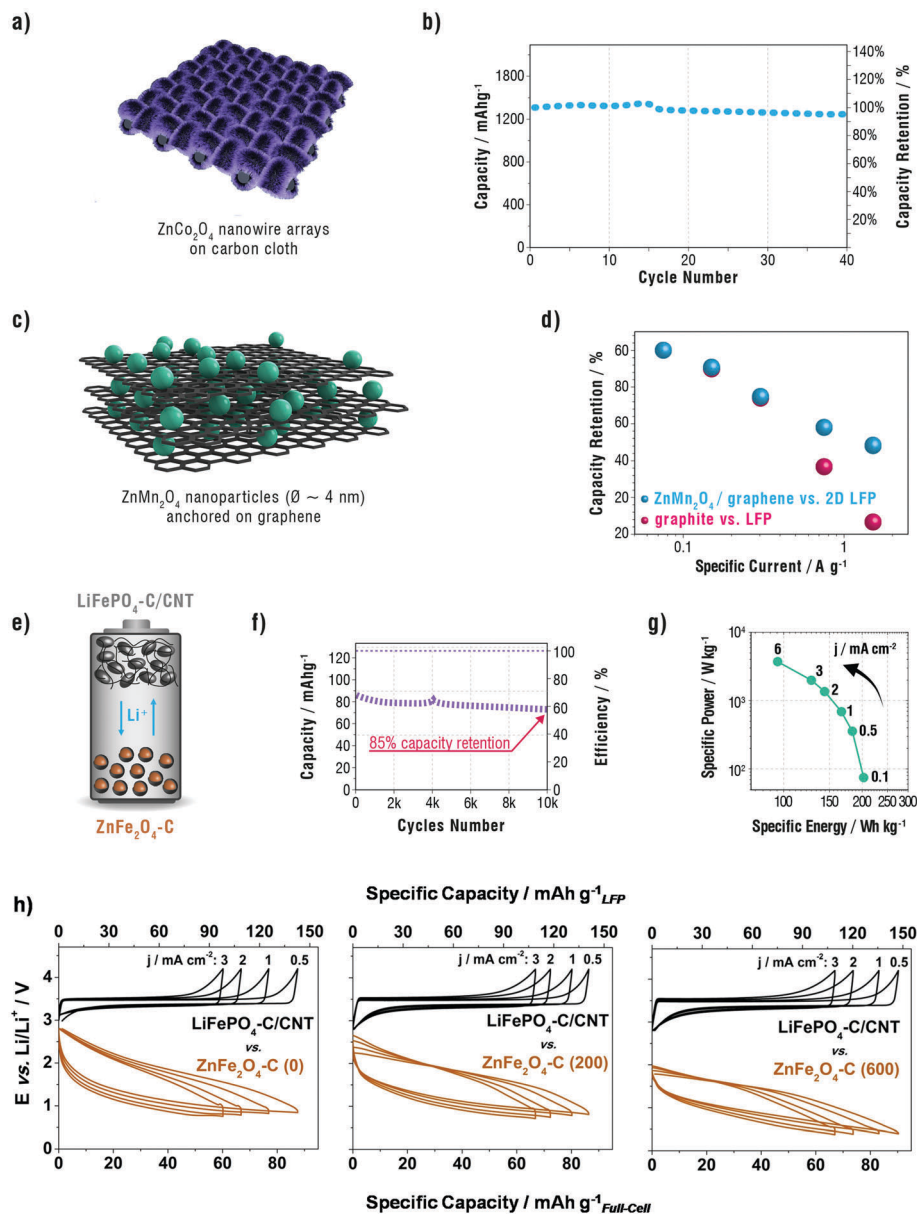
3356 | *Energy Environ. Sci.*, 2016, **9**, 3348–3367

This journal is © The Royal Society of Chemistry 2016

Fig. 5 Lithium-ion full-cell studies employing $ZnTM_2O_4$-based anodes: (a) Schematic illustration of $ZnCo_2O_4$ nanowire arrays deposited on carbon cloth, serving simultaneously as substrate and current collector, as reported by Liu et al.[165] and (b) its electrochemical performance, when coupled with a $LiCoO_2$-based cathode (2.2–3.7 V, 0.2 A g^{-1}). (c) Schematic illustration of the $ZnMn_2O_4$–graphene nanocomposite reported by Xiong et al.[151] and (d) its rate performance when combined with 2D LFP nanosheets as cathode (blue spheres; 0.9–3.9 V) in comparison with a standard lithium-ion full-cell including graphite and commercial LFP (red spheres). (e–h) Electrochemical performance of carbon-coated $ZnFe_2O_4$ nanoparticles in lithium-ion full-cell configuration vs. a LFP-C/CNT-based cathode as reported by Varzi et al.[166] (e) Schematic illustration of the prototype, (f) capacity vs. cycle number plot (4.2–2.8 and 2.8–0.05 V for the cathode and anode, respectively), (g) the corresponding Ragone-like plot (calculated on the base of the total active material content), and (h) the development of the $ZnFe_2O_4$-C anode (in brown) and LFP-C/CNT cathode (in black) voltage profiles when varying the degree of pre-full-cell-cycling lithium doping from fully delithiated (left) over 200 mA h g^{-1} (middle) to 600 mA h g^{-1} (right) at different current densities.

Accordingly, from a theoretical point of view, ZMO appears as the most suitable anode candidate. Nevertheless, the aforementioned full-cell studies also indicate that these materials are at present more suitable for high-power rather than for high-energy applications. Thus, the focus for further performance improvement may be set particularly on achieving enhanced rate capabilities and long-term cycling stability to position them as high-energy alternative for, e.g., lithium-ion supercapacitors (see also the previous section).

3.5 Binary transition metal oxides comprising tin

Though having received much less attention so far, also CAMs within which the electrochemically inactive TM was partially replaced by tin have been investigated. While the availability of tin may become an issue regarding its widespread implementation in large-scale batteries,[173,174] these materials offer further increased theoretical capacities due to the enhanced lithium storage capability of tin compared to zinc ($Li_{4.4}Sn$ vs. $LiZn$).[30,114]

This journal is © The Royal Society of Chemistry 2016

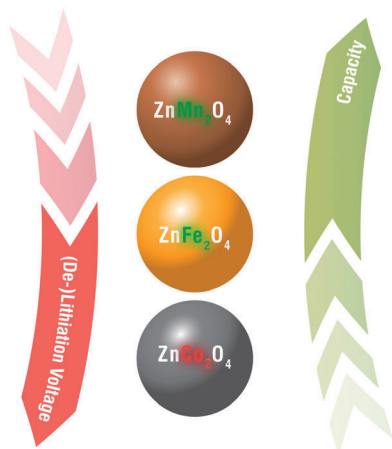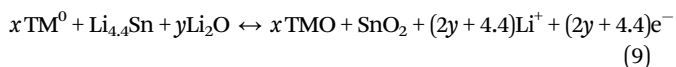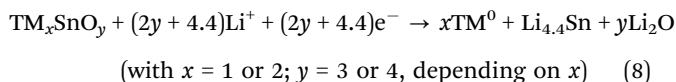Energy Environ. Sci., 2016, **9**, 3348–3367 | **3357**

Fig. 6 Schematic illustration of the impact of the comprised transition metal on the theoretical specific capacity and the (de-)lithiation voltage of $ZnTM_2O_4$ CAMs.

At present, mainly two different compounds were studied: TM_2SnO_4 (with TM = Co,[175–182] Ni,[183] or Mn[182,184,185]) and $TMSnO_3$ (with TM = Co[186–190] or Ni[191,192]). Depending on the comprised TM, spinel-structured TM_2SnO_4 and (frequently amorphous) $TMSnO_3$ offer specific capacities exceeding 1100 mA h g^{-1} and 1200 mA h g^{-1}, respectively (see Table 1), when considering the second step of the following reaction mechanism as fully reversible:

$$TM_xSnO_y + (2y + 4.4)Li^+ + (2y + 4.4)e^- \rightarrow xTM^0 + Li_{4.4}Sn + yLi_2O$$

$$\text{(with } x = 1 \text{ or } 2; y = 3 \text{ or } 4, \text{ depending on } x) \quad (8)$$

$$xTM^0 + Li_{4.4}Sn + yLi_2O \leftrightarrow xTMO + SnO_2 + (2y + 4.4)Li^+ + (2y + 4.4)e^- \quad (9)$$

In fact, the first studies on TM_2SnO_4 (TM = Co, Mn) in 2001[182] and 2002[175] introduced electrochemically inactive TMs into tin oxides as spectator ions to allow an X-ray-based correlation of the structural evolution to the occurring electrochemical processes for these commonly upon lithiation amorphized materials. Nevertheless, presumably related to the relatively low anodic cut-off potential of 2.0 V, they did not observe any direct evidence for a re-oxidation of the initially reduced metals.[175] This finding was challenged in 2003 by Huang et al.,[186] who proposed the reversible formation of CoO for a higher anodic cut-off potential of 3.0 V to explain at least part of the very high capacity, they obtained for $CoSnO_3$ ($\sim$1200 mA h g^{-1}). Further enhancing the understanding of the (de-)lithiation mechanism, Alcántara et al.[176] found that also tin is re-oxidized from Sn^0 to Sn^{4+} upon delithiation of Co_2SnO_4. The overall reaction mechanism, as given in (8) and (9), was then finally unraveled by performing ex situ high-resolution transmission electron microscopy (HRTEM) on (de-)lithiated $NiSnO_3$.[192] Concerning their utilization as lithium-ion anodes, however, these materials commonly suffer rapid capacity fading, which was assigned to the extensive volume changes and structural reorganization upon lithium uptake and release. As a matter of fact, the advantageous lithium storage capability of Sn compared to Zn is accompanied by a disadvantageous augmented volume variation.[181] It is interesting to note that, as a result, initially the conversion reaction (occurring at relatively higher voltages) becomes less reversible, later on followed by the alloying reaction.[180,190] This observation may be interpreted by a more pronounced sensitivity of the conversion reaction towards dramatic volume changes, which assumedly lead to the breakdown of the continuous, percolating electron conducting network.

To overcome these challenges, scientists followed mainly the same approaches as discussed for Zn-based CAMs (see examples presented in Table 2), including inter alia the incorporation of CNTs[178] or graphene.[180,190] For a Co_2SnO_4/graphene composite,[180] for instance, capacities of 800, 710, and 510 mA h g^{-1} were obtained when applying a specific current of 0.25, 0.5, and 1.0 A g^{-1}, respectively. Moreover, the authors reported a stable capacity of about 1090 mA h g^{-1} after 100 cycles at 0.1 A g^{-1}, assigning this very good performance to the enhanced structural integrity of the electrode composite, an increased electronic conductivity, and the reduced charge transfer resistance compared to the pure active material. Likewise, the application of carbonaceous surface coatings revealed substantial improvement,[177,179,185,187–189] in particular for coating thicknesses of 5–10 nm[177] and more,[188] as relatively thinner coatings (2–3 nm) did not provide a sufficient mechanic stability to buffer the extensive volume variations.[177] This approach did not only result in remarkable capacities of around 500 and 364 mA h g^{-1} for currents of 1.0 and 2.0 A g^{-1}, respectively,[188] but also in a stable capacity for 400 charge/ discharge cycles.[187]

Nonetheless, despite the larger theoretical capacities and decreased (de-)lithiation potentials,[175] the successful realization of long-term stable, high-performing lithium-ion anodes based on tin-comprising CAMs certainly makes even greater demands on scientists to develop advanced electrode architectures compared to Zn-comprising ones and research activities are currently still at an early stage.

4. From alloying to conversion/alloying

4.1 Enhancing the Li_2O conversion in alloying metal oxides

Within the previous section we have reviewed the approach of realizing CAMs by partially replacing the electrochemically inactive transition metal in conversion-type materials by a post-transition metal (PTM) like Zn or Sn, which can further alloy with lithium. As a result, substantially higher capacities and reduced lithium reaction voltages were realized (see also Table 1). In this section, we will now review the different opportunities of achieving a combined conversion/alloying mechanism when starting from the PTM oxides (PTMOs), thus, targeting further enhanced energy densities by increasing the relative contribution of the alloying reaction and lowering the (de-)lithiation potential.

The initial idea of utilizing alloying PTMOs, like SnO_2 or ZnO, rather than the pure metals was based on the concept that the in situ formed Li_2O (10) would serve as an electrochemically inactive matrix, buffering the occurring volume variations for

3358 | Energy Environ. Sci., 2016, 9, 3348–3367

This journal is © The Royal Society of Chemistry 2016

the subsequent (de-)alloying reaction (11) and acting as a glue for the thus formed PTM nanoparticles.[35–38] Nonetheless, the concomitant dramatic charge loss upon first lithiation ($\sim$48% for SnO_2 and $\sim$67% for ZnO) and, even more important, the fact that this matrix eventually does not prevent a continuous aggregation of metallic particles upon cycling,[37,193–199] resulting in a continuous capacity decay, has up to now precluded their application in commercial batteries.

$$PTMO_x + 2xLi^+ + 2xe^- \rightarrow PTM^0 + xLi_2O \quad (10)$$

$$PTM^0 + yLi^+ + ye^- \leftrightarrow Li_yPTM$$

$$\text{(with '}y\text{' depending on the PTM)} \quad (11)$$
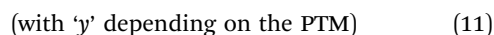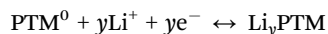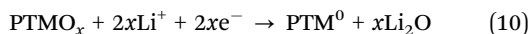
Nonetheless, both zinc oxide and particularly tin oxide[200] were studied extensively within the past years with respect to their reversible lithium storage capability. Remarkably, some of these studies[201–208] reported initial capacities exceeding the theoretical maxima for the alloying reaction only (329 mA h g^{-1} for ZnO and 782 mA h g^{-1} for SnO_2) when charging (delithiating) to sufficiently high anodic cut-off potentials. Considering the findings of Poizot et al.[39] and the suggestion of Courtney and Dahn,[37] that the Li_2O matrix may get decomposed above 1.3 V, it was proposed that also in these cases the partial re-oxidation of the PTM may be possible.[201–203] In fact, ex/in situ X-ray diffraction (XRD),[208–210] XPS,[208,211] and X-ray absorption spectroscopy (XAS)[197] studies later on confirmed the partial re-oxidation of PTM to $PTMO_x$, though only for the first cycle(s). With regard to the findings for pure conversion materials, reviewed in Section 2, it appears that the high diffusivity of the PTM in the Li_2O matrix and the resulting emergence of extremely large PTM particles (up to a few hundred nanometer)[193–199] inhibit the formation of a continuous percolating electronically conductive network, which is required for the degradation of Li_2O. However, it was also shown by in situ TEM that the application of, e.g., carbonaceous coatings can effectively suppress the formation of such large PTM crystals[212] and enhance the reversibility of the overall (de-)lithiation and, particularly, the conversion-type reaction (as indicated by the increased capacity at higher voltages).[55,56,213,214] As a result, nanoparticulate ZnO confined in a carbonaceous matrix,[214] for example, revealed a stable capacity of about 700 mA h g^{-1} for 200 cycles at 0.1 A g^{-1}. Similarly, ZnO/C nanorods coated with poly(3,4-ethylenedioxythiophene) polystyrene sulfonate (PEDOT–PSS)[210] showed a very impressive cycling stability, retaining a specific capacity of around 620 mA h g^{-1} after 1500 cycles applying a specific current of 0.98 A g^{-1}.

Nevertheless, it appears important to note that especially in case of Sn-based oxides, due to the substantially larger lithiation capacity and consequent volume expansion of tin, the confining coatings have to withstand an enormous mechanical strain, which in turn calls for sufficiently thick, i.e., stable coating layers.[212]

4.2 TM-doped ZnO and SnO_2

While the smart design of advanced active material composites incorporating electronically conductive secondary structures is apparently a successful way to enhance the conversion contribution in PTMOs, Bresser et al.[46] aimed for a more fundamental approach,

targeting the realization of an electron conducting network within the primary particles. To achieve this, they doped zinc oxide nanoparticles with electrochemically inactive transition metal (TM) cations, i.e., replaced part of the Zn cations by Fe or Co within the wurtzite lattice.[46,47] As a matter of fact, both compounds Fe- and Co-doped ZnO revealed dramatically improved reversible capacities compared to pure ZnO, up to the theoretically expected values of about 960 mA h g^{-1} ((12); see also Table 1 and Fig. 7a):

$$Zn_{1-x}TM_xO + (3-x)Li^+ + (3-x)e^- \rightarrow (1-x)LiZn + xTM^0 + Li_2O \quad (12)$$
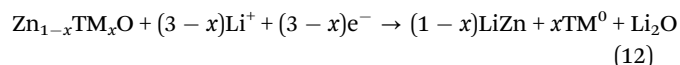
Intriguingly, Co-doped ZnO showed subsequently also a very stable cycling performance, while for Fe-doped ZnO the additional application of a carbonaceous coating, simultaneously interconnecting the single nanoparticles, appeared inevitable[46] (see also Table 2). Considering that both TMs commonly enable a very reversible conversion reaction (see Section 2), one possible reason for the diverging electrochemical performance may be the different oxidation state of the TM dopant – Fe^{3+} vs. Co^{2+} – as very recently revealed by Giuli et al.[47] who performed an in-depth structural characterization of these compounds. However, further studies will be required to affirm or negate a potential impact of the TM oxidation state on the electrochemical performance. Generally, the advantageous impact of the TM dopant, confirmed also by Yue et al.,[49] was assigned to an enhanced nanocrystallinity, i.e., the inhibition of extensive Zn crystal growth, in combination with a promoted LiZn alloying reaction as revealed by a comparative in situ XRD analysis of pristine and TM-doped ZnO.[46,48] In addition, the authors proposed that the electrochemically inactive TM nano-network ensures the required electron supply for the reduction of Li_2O throughout the primary particle.[46,48] In fact, there is a strong intercorrelation between these effects, as recently reported by Su et al.[198] They observed that the Zn crystal growth and the LiZn alloying reaction are current-dependent competitive processes. Accordingly, one may assume that – in addition to a constricting effect[215] – the percolating conductive TM network results in a relatively reduced current density, thus, kinetically favoring the alloying reaction rather than the zinc aggregation.

The general applicability of this approach was very recently corroborated by Mueller et al.[50] who performed an investigation on the influence of Fe-doping for SnO_2-based lithium-ion anodes. Indeed, a direct comparison of the potential profiles recorded for pure SnO_2 and Fe-doped SnO_2 (Fig. 7b) nicely illustrates the extended capacity gain at higher potentials, assigned to the deformation of Li_2O;[55] similarly, in fact, to an early study of Chen et al.[216] on iron oxide nanoparticles encased in hollow, submicron-sized SnO_2 spheres. Furthermore, capacity-limited cycling revealed also a beneficial impact of the Fe dopant on the reversibility of the alloying reaction, as reflected by a very stable performance at 600 mA h g^{-1} with high coulombic efficiency, similarly to a previous study on Mo-doped SnO_2.[217] Nevertheless, when (dis-)charging the electrodes in an extended voltage range (0.01 to 3.0 V), the (substantially higher) capacity gradually decreased, suggesting that further improvement by,
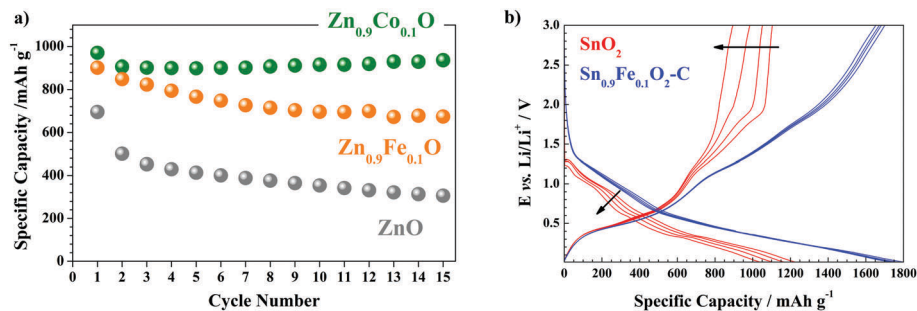
This journal is © The Royal Society of Chemistry 2016

Energy Environ. Sci., 2016, 9, 3348–3367 | 3359

Fig. 7 (a) Comparison of galvanostatically (dis-)charged electrodes comprising Co-doped (green), Fe-doped (orange), and pure ZnO (light grey) as active material (1st cycle: 0.024 A g^{-1}, following cycles: 0.048 A g^{-1}; electrode composition (active material : conductive carbon : binder): 75 : 20 : 5).[46] (b) Representative potential profiles (cycles 2–5) of alloying-type metal oxides (SnO_2 in red) and conversion/alloying-type binary metal oxides (carbon-coated $Sn_{0.9}Fe_{0.1}O_2$ in blue; as reported by Mueller *et al.*[50]) to depict the direct observation of an enhanced reversibility of the Li_2O formation by incorporating a TM (here: Fe) dopant (electrode composition see Table 2; note that the presented capacity for $Sn_{0.9}Fe_{0.1}O_2$-C is based solely on the content of $Sn_{0.9}Fe_{0.1}O_2$).

for instance, designing advanced electrode architectures[218] will have to be realized; similarly as for the Sn-based CAMs reviewed in Section 3.5, in fact.

4.3 Attaining the limits – transition metal silicates

With regard to the research efforts on pure alloying materials,[30,31] the target for developing new CAMs is certainly the incorporation of silicon. In addition to several general advantages – like its non-toxicity, environmental friendliness, and abundance – silicon provides a relatively low delithiation voltage ($\sim$0.4 V) and superior specific capacity (3578 mA h g^{-1} for $Li_{15}Si_4$), *i.e.*, the highest energy density after metallic lithium. Nonetheless, the accompanying extensive volume variations, leading to the loss of electronic contact, SEI instabilities, and, hence, continuous electrolyte decomposition, poor coulombic efficiency, and rapid capacity fading have so far hampered its practical application.[30,31] The realization of *in situ* formed ultrafine silicon nanograins, interconnected by a continuous network of highly conductive TM nanocrystals and embedded in a buffering matrix of, for instance, Li_2O – just like in CAMs – appears as a potential approach to overcome these challenges. However, to the best of our knowledge, no study on a silicon-comprising CAM has been reported, yet. In fact, the only class of silicon- and TM-based materials, investigated so far, is TM silicates (with TM being Ni,[219–221] Mn,[221–223] Fe,[221,224] Cu,[223,225] or Co[223,226,227] and binary combinations of these[221]). But despite stable specific capacities exceeding that of graphite, a surprisingly good rate capability even for micro-sized particles, *i.e.*, 477, 370, and 238 mA h g^{-1} for 0.8, 1.58, and 3.17 A g^{-1}, respectively,[226] and further enhanced performance by synthesizing advanced nanostructures[220,221,223,225,227] and/or incorporating secondary carbonaceous nanostructures,[220,222,227] no evidence for a successful reduction to elemental silicon and a reversible alloying reaction has been reported so far. Instead, complementary *ex/in situ* studies using electrochemical techniques, XRD, XPS, scanning electron microscopy (SEM), and HRTEM revealed the reduction of the TM to the metallic state and reversible formation of Li_4SiO_4[219,225,226] (13), accompanied by a partially reversible SEI formation.[226] In case of TM orthosilicates, this reaction may be summarized as follows:

$$TM_2SiO_4 + 4Li^+ + 4e^- \leftrightarrow 2TM^0 + Li_4SiO_4 \qquad (13)$$
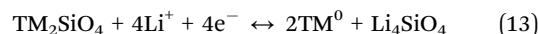
This finding is scientifically very interesting, as the formation of Li_4SiO_4 – in fact, a very good lithium ion conductor[228] – starting from silica was considered to be irreversible.[229,230] However, the theoretical capacity resulting from this reaction is rather limited (510 mA h g^{-1} for TM = Co, see also Table 1) and obtained along an entirely sloped potential profile,[226] rendering these materials at present unsuitable for high-energy lithium-ion batteries.

5. The (potential) advantages of CAMs

5.1 Comparison with conversion-type materials

Recapitulating the electrochemical properties of CAMs and the impact of combining conversion and alloying in a single compound, their advantages over pure conversion materials are immediately apparent. In fact, the introduction of an alloying element results in increased specific capacities, decreased average lithium reaction voltages, and reduced discharge/charge voltage hystereses, by this allowing for enhanced specific energies and energy storage efficiencies, *i.e.*, addressing simultaneously the two most important challenges of conversion-type anodes.

5.2 Comparison with alloying-type materials

Concerning the comparison with pure alloying materials, the advantages of CAMs may be less directly apparent. We may thus reconsider in a first step their major challenges and the two approaches to overcome these in already commercialized electrode composites. The greatest issue related to pure alloying materials is certainly the extensive volume variation upon lithium uptake/release, leading to substantial (anisotropic) mechanical stress, particularly in case of well-defined phase transitions. This is causing loss of electronic contact, electrode pulverization, and ongoing electrolyte decomposition due to continuously formed fresh surfaces.[30–34] To overcome this issue, the (nanoparticulate) electrochemically active alloying element is commonly embedded in a buffering matrix, which is ideally a good ionic and electronic conductor.[30] Nonetheless, the first industrial attempt in 1997 for realizing such alloying-type electrode composites using

3360 | *Energy Environ. Sci.*, 2016, **9**, 3348–3367

This journal is © The Royal Society of Chemistry 2016

tin-comprising glassy oxides[35] did eventually not reach the commercial stage due to the aggregation of the initially well dispersed tin upon continuous de-/lithiation and the large first cycle irreversibility required for forming the electrochemically inactive embedding matrix (see also Section 4.1).

In 2005, SONY successfully introduced a Sn–Co–C composite (presumably having a ratio of about 30 : 30 : 40), within which the cobalt/carbon matrix dilutes the occurring volume variation and prevents tin aggregation and crystallization upon de-/lithiation.[30,231–234] Interestingly, the role of cobalt appeared unique for the latter purpose, as revealed by extensive combinatorial studies including a variety of transition metals.[30,231–235] As a matter of fact, the same effect, that is the suppression of crystallite growth for the alloying element, is observed for the incorporation of a TM dopant (Fe or Co) in ZnO, i.e., Zn-based CAMs with an increased alloying contribution (Fig. 8); nevertheless, advantageously not limited to costly and toxic cobalt and for substantially lower TM contents (e.g., $Zn : TM = 10 : 1$).[46,48] With respect to the findings of Su et al.,[198] stating that the aggregation and alloying reaction would be two competing processes, the authors proposed that the presence of the metallic TM nano-network may, on the one hand, lead to an enhanced electronic conductivity throughout the initial primary particle and thus kinetically favor the alloying reaction and, on the other hand, physically hinder the diffusion of the alloying element nanocrystals[48] (see Section 4.2).

Beside the Sn–Co–C composite, also SiO_x ($x \approx 1$) is nowadays commercially employed as alloying-type active material, though only added in small percentage to graphite-based anodes.[15,30,236] The utilization of amorphous and understoichiometric silica, considered to be a dispersion of silicon grains in a SiO_2 matrix,[30,236] rather than silicon, follows mainly economic considerations, since SiO_x can be readily synthesized at large scale.[15,236] Additionally, the silica matrix, which is transformed to lithium silicate after the first lithiation,[30,229] serves as diluent for the occurring volume variations and as lithium ion conductor.[30,228] The associated irreversible lithium consumption, however, is the major issue for the addition of

larger percentages of SiO_x.[15,30] Remarkably, the most successful approach to decrease this initial irreversibility was reported by NEC researchers[237] who introduced metallic iron, nickel, or titanium into SiO_x thin film electrodes, thus, enhancing the first cycle coulombic efficiency from about 50% to more than 85%. According to an ex situ XPS analysis and the slightly sloped shape of the recorded potential profiles at higher voltages, this improved coulombic efficiency originated from the partially reversible formation of lithium oxide and/or lithium silicate. Notably, when further introducing metallic lithium, the authors were able to achieve first cycle coulombic efficiencies of about 100% and very stable cycling of lithium-ion full-cells. In fact, in the light of the herein reviewed CAMs and the underlying reaction mechanisms, these findings regarding the enhanced coulombic efficiency do not come as a surprise, but nicely highlight the potential advantages of alloying-rich CAMs over pure alloying-type compounds, i.e., enabling the reversibility of the conversion reaction by introducing a non-alloying element, as also observed for TM-doped ZnO and SnO_2 (see Section 4.2).

5.3 Summary of the (potential) advantages

Following the previous sections, it may be stated that CAMs – depending on their final composition and the applied voltage range – potentially address at the same time the remaining issues for pure conversion-type and those for the two already commercialized alloying-type active materials. Generally, CAMs provide a system that, as earlier considered ideal by Larcher et al.,[31] "generates in an in situ manner confined (ultrafine) metal nanoparticles", within which the nanocrystallinity of the alloying element is ensured by the non-alloying (transition) metal nano-network in combination with the surrounding amorphous lithium oxide.[35–38] As this combined matrix is commonly formed at slightly higher potentials compared to the alloying reaction, it effectively buffers the accompanying volume variation and ensures the electron[39,51,52] and ion transport[238,239] within the initial primary particles. Moreover, the initial capacity loss may be controlled by carefully selecting the anode delithiation voltage, though additional charge compensation, as described in Section 5.2 or at the end of Section 2, appears presently inevitable. Apart from all these rather mechanistic considerations, CAMs provide an additional advantage: Just like in case of SiO_x, the utilization of, for instance, oxides rather than pure metals or metalloids substantially facilitates their large-scale synthesis as well as the subsequent handling and processing at ambient atmosphere or in contact with a large variety of solvents; thus, offering potentially also the implementation of metals that are in its pure form highly reactive.

5.4 Remaining challenges

Despite all the (potential) intrinsic advantages of CAMs compared to pure conversion and alloying materials, there remain also some challenges for their application in commercial lithium-ion cells. First of all, even though the results reviewed herein show that the introduction of the alloying reaction leads to decreased de-/lithiation voltages and reduced voltage hystereses,
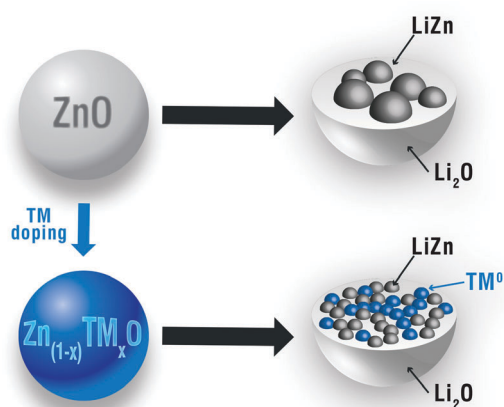

Fig. 8 Schematic illustration of the impact of introducing a TM dopant into ZnO on the lithiation mechanism and LiZn (Zn^0) crystallite growth according to the findings of Mueller et al.[48]

This journal is © The Royal Society of Chemistry 2016

Energy Environ. Sci., 2016, 9, 3348–3367 | 3361

further improvement is certainly required to enhance the overall energy storage efficiency and avoid internal heat evolution, *i.e.*, avoid any potential safety issue with regard to the implementation of such compounds. Comparative studies, investigating pure conversion materials and the corresponding CAMs with a step-wise increase of the alloying element ratio by means of sophisticated electrochemical techniques at (near-to) equilibrium conditions like, for instance, the galvanostatic intermittent titration technique (GITT) or the potentiostatic intermittent titration technique (PITT), may provide further insight into this issue. Moreover, the smart design of new CAMs, using suitable transition and post-transition metal cation/anion combinations and by this modifying the de-/lithiation reaction pathways and redox potentials is anticipated to result in substantial progress (as also elaborated in more detail in the following paragraph).

The latter approach may, indeed, eventually help also to overcome the second main challenge, the relatively higher voltage of the conversion reaction, limiting its accessibility in practical lithium-ion full-cells. The implementation of suitable transition metals, re-oxidizing at relatively low potentials (*e.g.*, Mn or Cr), may provide a suitable way in this regard. However, this will have to be accompanied by an enhanced understanding of the interplay of the transition metal redox process and that of the lithiated species. Considering the findings reviewed and discussed herein, it appears favorable to ensure a highly homogeneous distribution of these two compounds in the lithiated state, ideally characterized by ultrafine grain-sizes and highly percolating networks, while at the same time providing a sufficiently high mechanical stability to prevent the crystallite growth of the alloying element. The realization and, in fact, also the investigation of this task is certainly very challenging, but the rapid development in recent years of advanced characterization techniques such as *in situ* TEM and XAS gives rise to optimism that overcoming these challenges is possible.

The third and last major challenge is not directly related to the materials itself, but to its impact on the electrochemical stability of the electrolyte. In fact, the success of the state-of-the-art anode material graphite is a result of the finding that ethylene carbonate forms a stable SEI on its surface, thus preventing a continuous electrolyte degradation.[240] As discussed earlier, the application of carbonaceous coatings targets in this direction and promising results were reported. Nevertheless, the development of an in-depth comprehension of the impact of the chemical nature of the electrode, the exposed crystallite facets, and the composition of the electrolyte may help to address this issue from a fundamental perspective – though the still remaining questions concerning the SEI on graphite render such a systematic investigation a more than extensive research project. Potentially – just like in the case of graphite – the development of new electrolyte systems will eventually enable a stabilized electrode/electrolyte interface.

6. Conclusions and perspectives

Apparently, great progress has been achieved in the rather young research field of CAMs. Materials like $ZnTM_2O_4$, which were initially considered to be electrochemically inactive, turned out

to be highly suitable for long-life and high-power LIBs when carefully designing advanced electrode architectures, including *inter alia* carbonaceous coatings or graphene-based matrices. Also for tin-based CAMs and PTMOs continuously improving performances are reported thanks to the steadily increasing ability of researchers to develop nanostructured hierarchical composites. This rapid progress benefits largely from the great achievements obtained for pure alloying- or conversion-type compounds and the general ability to tailor materials' properties, morphologies, and interactions on the nanoscale.

However, though these composite design strategies are indispensable for realizing high-performance CAM anodes, it appears that particularly the further decrease of the lithium reaction potential and the voltage hysteresis, *i.e.*, the energy density and energy efficiency, respectively, require an optimization of the materials itself, thus, on the atomic scale rather than on the nanoscale. Therefore, an in-depth understanding of the detailed reaction mechanisms upon (de-)lithiation in an electrochemical cell is needed. Nonetheless, based on the insights into pure conversion- and alloying-type compounds, TM-doped PTMOs were developed, showing great promises in this regard, and it is anticipated that further enhancement can be realized by carefully selecting the incorporated TM and PTM cations. The utilization of manganese, for instance, as TM commonly results in relatively low average lithium reaction voltages, as summarized in Table 1.

With respect to the choice of the PTM, zinc certainly has some advantages concerning its availability,[174] non-toxicity, and relatively small volume variation upon (de-)lithiation, *i.e.*, volumetric energy density when considering the lithiated state of the anode;[30] nevertheless, at the expense of less gravimetric capacity compared to tin. As an alternative, germanium with a theoretical capacity of 1385 mA h g^{-1} ($\hat{=}Li_{15}Ge_4$[241]), low delithiation voltage of about 0.5 V, and fast lithium diffusion[242] would be very promising, in particular, as it has shown a remarkably stable cycling, both in its metallic[242,243] as well as in its oxide form,[54,244] but its high cost limits its use to niche applications like, for example, space or military applications. Generally, every element, which can reversibly alloy with lithium, appears conceivable to be employed in new CAMs,[30–34] but, particularly with respect to its natural abundance, the final target is certainly silicon. In fact, even if not analyzed or discussed by the authors,[223] the potential profiles reported for cobalt silicate hollow spheres (Section 4.3) revealed some alloying-like characteristics in the low-voltage region. This observation and the findings of Miyachi *et al.*,[237] regarding the partial reversibility of lithium oxide and/or lithium silicate when introducing metallic iron, nickel, or titanium into SiO_x thin film electrodes (see Section 5.2), provide hope that silicon-based CAMs may, indeed, be realized. We may briefly note at this point that the selection of the alloying element should focus not only on the gravimetric capacity but also keeping in mind the volumetric values, comprehensibly summarized and reasoned very recently by Obrovac and Chevrier,[30] which are especially important for small-scale LIBs for portable electronic devices.[15]

Another option to tailor the (de-)lithiation voltage and enhance the energy storage efficiency concerns the variation

3362 | *Energy Environ. Sci.*, 2016, **9**, 3348–3367

This journal is © The Royal Society of Chemistry 2016

of the anion. According to Aymard and co-workers,[69] the voltage hysteresis decreases in the order fluorides > oxides > sulfides > nitrides > phosphides > hydrides. Moreover, switching from oxides to nitrides or phosphides, for instance, may lead to improved power performances with respect to the high ionic conductivity of the resulting lithium species.[245–248]

As a result, an almost unlimited number of possible (multi-)cation/(multi-)anion combinations, each characterized by defined lithium reaction voltages and specific capacities appears conceivable.

Acknowledgements

References

1 J.-M. Tarascon and M. Armand, *Nature*, 2001, **414**, 359–367.
2 T. Horiba, T. Maeshima, T. Matsumura, M. Koseki, J. Arai and Y. Muranaka, *J. Power Sources*, 2005, **146**, 107–110.
3 J. Weinert, J. Ogden, D. Sperling and A. Burke, *Energy Policy*, 2008, **36**, 2544–2555.
4 B. Scrosati and J. Garche, *J. Power Sources*, 2010, **195**, 2419–2430.
5 M. Armand and J.-M. Tarascon, *Nature*, 2008, **451**, 652–657.
6 J. Tollefson, *Nature*, 2008, **456**, 436–440.
7 B. Scrosati, J. Hassoun and Y.-K. Sun, *Energy Environ. Sci.*, 2011, **4**, 3287–3295.
8 O. van Vliet, A. S. Brouwer, T. Kuramochi, M. van den Broek and A. Faaij, *J. Power Sources*, 2011, **196**, 2298–2310.
9 M. M. Thackeray, C. Wolverton and E. D. Isaacs, *Energy Environ. Sci.*, 2012, **5**, 7854–7863.
10 P. G. Bruce, S. A. Freunberger, L. J. Hardwick and J.-M. Tarascon, *Nat. Mater.*, 2012, **11**, 19–29.
11 D. Bresser, S. Passerini and B. Scrosati, *Chem. Commun.*, 2013, **49**, 10545–10562.
12 A. Manthiram, Y. Fu, S.-H. Chung, C. Zu and Y.-S. Su, *Chem. Rev.*, 2014, **114**, 11751–11787.
13 A. C. Luntz and B. D. McCloskey, *Chem. Rev.*, 2014, **114**, 11721–11750.
14 L. Grande, E. Paillard, J. Hassoun, J.-B. Park, Y.-J. Lee, Y.-K. Sun, S. Passerini and B. Scrosati, *Adv. Mater.*, 2015, **27**, 784–800.
15 J. W. Choi and D. Aurbach, *Nat. Rev. Mater.*, 2016, **1**, 16013.
16 P. C. Howlett, D. R. MacFarlane and A. F. Hollenkamp, *Electrochem. Solid-State Lett.*, 2004, **7**, A97–A101.
17 S. Seki, Y. Kobayashi, H. Miyashiro, Y. Ohno, Y. Mita, A. Usami, N. Terada and M. Watanabe, *Electrochem. Solid-State Lett.*, 2005, **8**, A577–A578.
18 M. Gauthier, A. Bélanger, P. Bouchard, B. Kapfer, S. Ricard, G. Vassort, M. Armand, J. Y. Sanchez and L. Krause, *J. Power Sources*, 1995, **54**, 163–169.
19 R. Bouchet, S. Maria, R. Meziane, A. Aboulaich, L. Lienafa, J.-P. Bonnet, T. N. T. Phan, D. Bertin, D. Gigmes, D. Devaux, R. Denoyel and M. Armand, *Nat. Mater.*, 2013, **12**, 452–457.
20 M. Kotobuki, H. Munakata, K. Kanamura, Y. Sato and T. Yoshida, *J. Electrochem. Soc.*, 2010, **157**, A1076–A1079.
21 K. Takada, *Acta Mater.*, 2013, **61**, 759–770.
22 G. Zheng, S. W. Lee, Z. Liang, H.-W. Lee, K. Yan, H. Yao, H. Wang, W. Li, S. Chu and Y. Cui, *Nat. Nanotechnol.*, 2014, **9**, 618–623.
23 W. Xu, J. Wang, F. Ding, X. Chen, E. Nasybulin, Y. Zhang and J.-G. Zhang, *Energy Environ. Sci.*, 2014, **7**, 513–537.
24 Y. Yang, M. T. McDowell, A. Jackson, J. J. Cha, S. S. Hong and Y. Cui, *Nano Lett.*, 2010, **10**, 1486–1491.
25 J. Hassoun, H.-G. Jung, D.-J. Lee, J.-B. Park, K. Amine, Y.-K. Sun and B. Scrosati, *Nano Lett.*, 2012, **12**, 5775–5779.
26 R. Elazari, G. Salitra, G. Gershinsky, A. Garsuch, A. Panchenko and D. Aurbach, *Electrochem. Commun.*, 2012, **14**, 21–24.
27 G. Cohn, D. Starosvetsky, R. Hagiwara, D. D. Macdonald and Y. Ein-Eli, *Electrochem. Commun.*, 2009, **11**, 1916–1918.
28 J. Hassoun and B. Scrosati, *Angew. Chem., Int. Ed.*, 2010, **49**, 2371–2374.
29 G. A. Elia, D. Bresser, J. Reiter, P. Oberhumer, Y.-K. Sun, B. Scrosati, S. Passerini and J. Hassoun, *ACS Appl. Mater. Interfaces*, 2015, **7**, 22638–22643.
30 M. N. Obrovac and V. L. Chevrier, *Chem. Rev.*, 2014, **114**, 11444–11502.
31 D. Larcher, S. Beattie, M. Morcrette, K. Edstrom, J.-C. Jumas and J.-M. Tarascon, *J. Mater. Chem.*, 2007, **17**, 3759–3772.
32 C.-M. Park, J.-H. Kim, H. Kim and H.-J. Sohn, *Chem. Soc. Rev.*, 2010, **39**, 3115–3141.
33 W.-J. Zhang, *J. Power Sources*, 2011, **196**, 13–24.
34 N. Nitta and G. Yushin, *Part. Part. Syst. Charact.*, 2014, **31**, 317–336.
35 Y. Idota, T. Kubota, A. Matsufuji, Y. Maekawa and T. Miyasaka, *Science*, 1997, **276**, 1395–1397.
36 I. A. Courtney and J. R. Dahn, *J. Electrochem. Soc.*, 1997, **144**, 2045–2052.
37 I. A. Courtney and J. R. Dahn, *J. Electrochem. Soc.*, 1997, **144**, 2943–2948.
38 R. A. Huggins, *Ionics*, 1997, **3**, 245–255.
39 P. Poizot, S. Laruelle, S. Grugeon, L. Dupont and J.-M. Tarascon, *Nature*, 2000, **407**, 496–499.
40 M. R. Palacin, *Chem. Soc. Rev.*, 2009, **38**, 2565–2575.
41 J. Cabana, L. Monconduit, D. Larcher and M. R. Palacín, *Adv. Mater.*, 2010, **22**, E170–E192.
42 M. V. Reddy, G. V. Subba Rao and B. V. R. Chowdari, *Chem. Rev.*, 2013, **113**, 5364–5457.
43 C. Yuan, H. B. Wu, Y. Xie and X. W. (David) Lou, *Angew. Chem., Int. Ed.*, 2014, **53**, 1488–1504.
44 N. Loeffler, D. Bresser, S. Passerini and M. Copley, *Johnson Matthey Technol. Rev.*, 2015, **59**, 34–44.
45 P. L. Taberna, S. Mitra, P. Poizot, P. Simon and J.-M. Tarascon, *Nat. Mater.*, 2006, **5**, 567–573.
46 D. Bresser, F. Mueller, M. Fiedler, S. Krueger, R. Kloepsch, D. Baither, M. Winter, E. Paillard and S. Passerini, *Chem. Mater.*, 2013, **25**, 4977–4985.

This journal is © The Royal Society of Chemistry 2016

Energy Environ. Sci., 2016, **9**, 3348–3367 | 3363

47 G. Giuli, A. Trapananti, F. Mueller, D. Bresser, F. d'Acapito and S. Passerini, *Inorg. Chem.*, 2015, **54**, 9393–9400.

48 F. Mueller, D. Geiger, U. Kaiser, S. Passerini and D. Bresser, *ChemElectroChem*, 2016, **3**, 1311–1319.

49 H. Yue, Z. Shi, Q. Wang, Z. Cao, H. Dong, Y. Qiao, Y. Yin and S. Yang, *ACS Appl. Mater. Interfaces*, 2014, **6**, 17067–17074.

50 F. Mueller, D. Bresser, V. S. K. Chakrayadhanula and S. Passerini, *J. Power Sources*, 2015, **299**, 398–402.

51 F. Wang, R. Robert, N. A. Chernova, N. Pereira, F. Omenya, F. Badway, X. Hua, M. Ruotolo, R. Zhang, L. Wu, V. Volkov, D. Su, B. Key, M. S. Whittingham, C. P. Grey, G. G. Amatucci, Y. Zhu and J. Graetz, *J. Am. Chem. Soc.*, 2011, **133**, 18828–18836.

52 F. Wang, H.-C. Yu, M.-H. Chen, L. Wu, N. Pereira, K. Thornton, A. van der Ven, Y. Zhu, G. G. Amatucci and J. Graetz, *Nat. Commun.*, 2012, **3**, 1201.

53 F. Lin, D. Nordlund, T.-C. Weng, Y. Zhu, C. Ban, R. M. Richards and H. L. Xin, *Nat. Commun.*, 2014, **5**, 3358.

54 K. H. Seng, M. Park, Z. P. Guo, H. K. Liu and J. Cho, *Nano Lett.*, 2013, **13**, 1230–1236.

55 X. W. Guo, X. P. Fang, Y. Sun, L. Y. Shen, Z. X. Wang and L. Q. Chen, *J. Power Sources*, 2013, **226**, 75–81.

56 S. J. Yang, S. Nam, T. Kim, J. H. Im, H. Jung, J. H. Kang, S. Wi, B. Park and C. R. Park, *J. Am. Chem. Soc.*, 2013, **135**, 7394–7397.

57 D. W. Murphy and P. A. Christian, *Science*, 1979, **205**, 651–656.

58 R. Dedryvère, S. Laruelle, S. Grugeon, P. Poizot, D. Gonbeau and J.-M. Tarascon, *Chem. Mater.*, 2004, **16**, 1056–1061.

59 Q. Su, J. Zhang, Y. Wu and G. Du, *Nano Energy*, 2014, **9**, 264–272.

60 H. Wang, L.-F. Cui, Y. Yang, H. Sanchez Casalongue, J. T. Robinson, Y. Liang, Y. Cui and H. Dai, *J. Am. Chem. Soc.*, 2010, **132**, 13978–13980.

61 S. Grugeon, S. Laruelle, L. Dupont, F. Chevallier, P. L. Taberna, P. Simon, L. Gireaud, S. Lascaud, E. Vidal, B. Yrieix and M. Tarascon, *Chem. Mater.*, 2005, **17**, 5041–5047.

62 P. Meduri, E. Clark, J. H. Kim, E. Dayalan, G. U. Sumanasekera and M. K. Sunkara, *Nano Lett.*, 2012, **12**, 1784–1788.

63 P. Balaya, H. Li, L. Kienle and J. Maier, *Adv. Funct. Mater.*, 2003, **13**, 621–625.

64 W.-J. Li and Z.-W. Fu, *Appl. Surf. Sci.*, 2010, **256**, 2447–2452.

65 K. Chang and W. Chen, *Chem. Commun.*, 2011, **47**, 4252–4254.

66 N. Pereira, L. Dupont, J. M. Tarascon, L. C. Klein and G. G. Amatucci, *J. Electrochem. Soc.*, 2003, **150**, A1273–A1280.

67 H. Li, P. Balaya and J. Maier, *J. Electrochem. Soc.*, 2004, **151**, A1878–A1885.

68 V. Pralong, D. C. S. Souza, K. T. Leung and L. F. Nazar, *Electrochem. Commun.*, 2002, **4**, 516–520.

69 Y. Oumellal, A. Rougier, G. A. Nazri, J.-M. Tarascon and L. Aymard, *Nat. Mater.*, 2008, **7**, 916–921.

70 M. J. Aragón, C. Pérez-Vicente and J. L. Tirado, *Electrochem. Commun.*, 2007, **9**, 1744–1748.

71 Y. Sharma, N. Sharma, G. V. S. Rao and B. V. R. Chowdari, *J. Mater. Chem.*, 2009, **19**, 5047–5054.

72 N. Tian, C. Hua, Z. Wang and L. Chen, *J. Mater. Chem. A*, 2015, **3**, 14173–14177.

73 A. Debart, L. Dupont, P. Poizot, J.-B. Leriche and J. M. Tarascon, *J. Electrochem. Soc.*, 2001, **148**, A1266–A1274.

74 L. Li, F. Meng and S. Jin, *Nano Lett.*, 2012, **12**, 6030–6037.

75 D. A. Porter, K. E. Easterling and M. Y. Sherif, *Phase Transformations in Metals and Alloys*, CRC Press, Taylor & Francis Group, Boca Raton, London, New York, 3rd edn, 2009.

76 K. E. Gregorczyk, Y. Liu, J. P. Sullivan and G. W. Rubloff, *ACS Nano*, 2013, **7**, 6354–6360.

77 D. Bresser, E. Paillard, P. Niehoff, S. Krueger, F. Mueller, M. Winter and S. Passerini, *ChemPhysChem*, 2014, **15**, 2177–2185.

78 O. Delmer, P. Balaya, L. Kienle and J. Maier, *Adv. Mater.*, 2008, **20**, 501–505.

79 J.-M. Tarascon, S. Grugeon, M. Morcrette, S. Laruelle, P. Rozier and P. Poizot, *C. R. Chim.*, 2005, **8**, 9–15.

80 C. N. R. Rao, *Annu. Rev. Phys. Chem.*, 1989, **40**, 291.

81 K. Hübner and G. Leonhardt, *Phys. Status Solidi B*, 1975, **68**, K175–K179.

82 F. Mestre-Aizpurua, S. Laruelle, S. Grugeon, J.-M. Tarascon and M. R. Palacín, *J. Appl. Electrochem.*, 2010, **40**, 1365–1370.

83 F.-X. Ma, H. Hu, H. B. Wu, C.-Y. Xu, Z. Xu, L. Zhen and X. W. (David) Lou, *Adv. Mater.*, 2015, **27**, 4097–4101.

84 N. Du, H. Zhang, B. D. Chen, J. B. Wu, X. Y. Ma, Z. H. Liu, Y. Q. Zhang, D. R. Yang, X. H. Huang and J. P. Tu, *Adv. Mater.*, 2007, **19**, 4505–4509.

85 W. Yue, Z. Lin, S. Jiang and X. Yang, *J. Mater. Chem.*, 2012, **22**, 16318–16323.

86 Y. Ma, C.-W. Tai, R. Younesi, T. Gustafsson, J. Y. Lee and K. Edström, *Chem. Mater.*, 2015, **27**, 7698–7709.

87 M. R. Tarasevich and B. N. Efremov, *Electrodes of Conductive Metal Oxides, Part A*, Elsevier Scientific Publishing Co., Amsterdam, NL, New York, USA, 1980.

88 L. Zhang, H. B. Wu and X. W. (David) Lou, *Adv. Energy Mater.*, 2014, **4**, 1300958.

89 R. E. Doe, K. A. Persson, Y. S. Meng and G. Ceder, *Chem. Mater.*, 2008, **20**, 5274–5283.

90 L. Su, Z. Zhou and P. Shen, *J. Phys. Chem. C*, 2012, **116**, 23974–23980.

91 L. Su, Y. Zhong and Z. Zhou, *J. Mater. Chem. A*, 2013, **1**, 15158–15166.

92 S. Laruelle, S. Grugeon, P. Poizot, M. Dollé, L. Dupont and J.-M. Tarascon, *J. Electrochem. Soc.*, 2002, **149**, A627–A634.

93 S. Grugeon, S. Laruelle, L. Dupont and J.-M. Tarascon, *Solid State Sci.*, 2003, **5**, 895–904.

94 A. Ponrouch, P.-L. Taberna, P. Simon and M. R. Palacín, *Electrochim. Acta*, 2012, **61**, 13–18.

95 J. Zhang, R. Wang, X. Yang, W. Lu, X. Wu, X. Wang, H. Li and L. Chen, *Nano Lett.*, 2012, **12**, 2153–2157.

96 L. Martin, H. Martinez, D. Poinot, B. Pecquenard and F. Le Cras, *J. Power Sources*, 2014, **248**, 861–873.

97 A. S. Aricò, P. Bruce, B. Scrosati, J. M. Tarascon and W. van Schalkwijk, *Nat. Mater.*, 2005, **4**, 366–377.

98 S. A. Needham, G. X. Wang, K. Konstantinov, Y. Tournayre, Z. Lao and H. K. Liu, *Electrochem. Solid-State Lett.*, 2006, **9**, A315–A319.

3364 | *Energy Environ. Sci.*, 2016, **9**, 3348–3367

This journal is © The Royal Society of Chemistry 2016

99 R. G. Pearson, *J. Am. Chem. Soc.*, 1963, **85**, 3533–3539.

100 R. G. Pearson, *J. Chem. Educ.*, 1968, **45**, 581.

101 V. Aravindan, Y.-S. Lee and S. Madhavi, *Adv. Energy Mater.*, 2015, **5**, 1402225.

102 J. Ming, W. J. Kwak, S. J. Youn, H. Ming, J. Hassoun and Y.-K. Sun, *Energy Technol.*, 2014, **2**, 778–785.

103 A. Suryawanshi, V. Aravindan, D. Mhamane, P. Yadav, S. Patil, S. Madhavi and S. Ogale, *Energy Storage Mater*, 2015, **1**, 152–157.

104 F. Badway, I. Plitz, S. Grugeon, S. Laruelle, M. Dollé, A. S. Gozdz and J.-M. Tarascon, *Electrochem. Solid-State Lett.*, 2002, **5**, A115–A118.

105 D. Shanmukaraj, S. Grugeon, S. Laruelle, G. Douglade, J.-M. Tarascon and M. Armand, *Electrochem. Commun.*, 2010, **12**, 1344–1347.

106 C. R. Jarvis, M. J. Lain, M. V. Yakovleva and Y. Gao, *J. Power Sources*, 2006, **162**, 800–802.

107 X. Fan, Y. Zhu, C. Luo, L. Suo, Y. Lin, T. Gao, K. Xu and C. Wang, *ACS Nano*, 2016, **10**, 5567–5577.

108 G. Zhou, D.-W. Wang, F. Li, L. Zhang, N. Li, Z.-S. Wu, L. Wen, G. Q. (Max) Lu and H.-M. Cheng, *Chem. Mater.*, 2010, **22**, 5306–5313.

109 J. O. Besenhard, J. Yang and M. Winter, *J. Power Sources*, 1997, **68**, 87–90.

110 M. Winter and J. O. Besenhard, *Electrochim. Acta*, 1999, **45**, 31–50.

111 S. Grugeon, S. Laruelle, R. Herrera-Urbina, L. Dupont, P. Poizot and J.-M. Tarascon, *J. Electrochem. Soc.*, 2001, **148**, A285–A292.

112 Q. Chen and K. Sieradzki, *Nat. Mater.*, 2013, **12**, 1102–1106.

113 A. Kushima, X. H. Liu, G. Zhu, Z. L. Wang, J. Y. Huang and J. Li, *Nano Lett.*, 2011, **11**, 4535–4541.

114 A. N. Dey, *J. Electrochem. Soc.*, 1971, **118**, 1547–1549.

115 C. J. Chen, M. Greenblatt and J. V. Waszczak, *Solid State Ionics*, 1986, **18–19**(2), 838–846.

116 Y.-N. NuLi, Y.-Q. Chu and Q.-Z. Qin, *J. Electrochem. Soc.*, 2004, **151**, A1077–A1083.

117 Y. Sharma, N. Sharma, G. V. S. Rao and B. V. R. Chowdari, *Electrochim. Acta*, 2008, **53**, 2380–2385.

118 X. Guo, X. Lu, X. Fang, Y. Mao, Z. Wang, L. Chen, X. Xu, H. Yang and Y. Liu, *Electrochem. Commun.*, 2010, **12**, 847–850.

119 Z. Xing, Z. Ju, J. Yang, H. Xu and Y. Qian, *Nano Res.*, 2012, **5**, 477–485.

120 C. Ai, M. Yin, C. Wang and J. Sun, *J. Mater. Sci.*, 2004, **39**, 1077–1079.

121 Y. Yang, Y. Zhao, L. Xiao and L. Zhang, *Electrochem. Commun.*, 2008, **10**, 1117–1120.

122 Y. Sharma, N. Sharma, G. V. Subba Rao and B. V. R. Chowdari, *Adv. Funct. Mater.*, 2007, **17**, 2855–2861.

123 N. Du, Y. Xu, H. Zhang, J. Yu, C. Zhai and D. Yang, *Inorg. Chem.*, 2011, **50**, 3320–3324.

124 S.-W. Kim, H.-W. Lee, P. Muralidharan, D.-H. Seo, W.-S. Yoon, D. Kim and K. Kang, *Nano Res.*, 2011, **4**, 505–510.

125 Y. Qiu, S. Yang, H. Deng, L. Jin and W. Li, *J. Mater. Chem.*, 2010, **20**, 4439–4444.

126 M. S. Song, Y. J. Cho, D. Y. Yoon, S. Nahm, S. H. Oh, K. Woo, J. M. Ko and W. I. Cho, *Electrochim. Acta*, 2014, **137**, 266–272.

127 P. F. Teh, Y. Sharma, S. S. Pramana and M. Srinivasan, *J. Mater. Chem.*, 2011, **21**, 14999–15008.

128 N. Wang, X. Ma, H. Xu, L. Chen, J. Yue, F. Niu, J. Yang and Y. Qian, *Nano Energy*, 2014, **6**, 193–199.

129 X. Hou, X. Wang, L. Yao, S. Hu, Y. Wu and X. Liu, *New J. Chem.*, 2015, **39**, 1943–1952.

130 X.-B. Zhong, Z.-Z. Yang, H.-Y. Wang, L. Lu, B. Jin, M. Zha and Q.-C. Jiang, *J. Power Sources*, 2016, **306**, 718–723.

131 Y. Deng, Q. Zhang, S. Tang, L. Zhang, S. Deng, Z. Shi and G. Chen, *Chem. Commun.*, 2011, **47**, 6828–6830.

132 K. Wang, Y. Huang, D. Wang, Y. Zhao, M. Wang, X. Chen, X. Qin and S. Li, *RSC Adv.*, 2015, **5**, 107247.

133 L. Zhou, H. B. Wu, T. Zhu and X. W. (David) Lou, *J. Mater. Chem.*, 2012, **22**, 827–829.

134 J. Bai, X. Li, G. Liu, Y. Qian and S. Xiong, *Adv. Funct. Mater.*, 2014, **24**, 3012–3020.

135 J. M. Won, S. H. Choi, Y. J. Hong, Y. N. Ko and Y. C. Kang, *Sci. Rep.*, 2014, **4**, 5857.

136 G. Zhang, L. Yu, H. B. Wu, H. E. Hoster and X. W. (David) Lou, *Adv. Mater.*, 2012, **24**, 4609–4613.

137 L.-X. Zhang, Y.-L. Wang, H.-F. Jiu, H. Qiu and H. Wang, *Ceram. Int.*, 2015, **41**, 9655–9661.

138 L. Hou, L. Lian, L. Zhang, G. Pang, C. Yuan and X. Zhang, *Adv. Funct. Mater.*, 2015, **25**, 238–246.

139 F. Zou, X. Hu, Z. Li, L. Qie, C. Hu, R. Zeng, Y. Jiang and Y. Huang, *Adv. Mater.*, 2014, **26**, 6622–6628.

140 D. Zhao, Y. Xiao, X. Wang, Q. Gao and M. Cao, *Nano Energy*, 2014, **7**, 124–133.

141 R. Wu, X. Qian, K. Zhou, J. Wei, J. Lou and P. M. Ajayan, *ACS Nano*, 2014, **8**, 6297–6303.

142 X.-B. Zhong, B. Jin, Z.-Z. Yang, C. Wang and H.-Y. Wang, *RSC Adv.*, 2014, **4**, 55173–55178.

143 L. Yao, X. Hou, S. Hu, X. Tang, X. Liu and Q. Ru, *J. Alloys Compd.*, 2014, **585**, 398–403.

144 J. Sui, C. Zhang, D. Hong, J. Li, Q. Cheng, Z. Li and W. Cai, *J. Mater. Chem.*, 2012, **22**, 13674–13681.

145 P. Li, J. Liu, J. Liu, Y. Wang, Z. Li, W. Wu, Y. Wang, L. Yin, H. Xie, M. Wu, X. He and J. Qiu, *Electrochim. Acta*, 2015, **180**, 164–172.

146 L. Yin, Z. Zhang, Z. Li, F. Hao, Q. Li, C. Wang, R. Fan and Y. Qi, *Adv. Funct. Mater.*, 2014, **24**, 4176–4185.

147 X. Yao, J. Kong, D. Zhou, C. Zhao, R. Zhou and X. Lu, *Carbon*, 2014, **79**, 493–499.

148 Y. Dong, Y. Xia, Y.-S. Chui, C. Cao and J. A. Zapien, *J. Power Sources*, 2015, **275**, 769–776.

149 P. Xiong, B. Liu, V. Teran, Y. Zhao, L. Peng, X. Wang and G. Yu, *ACS Nano*, 2014, **8**, 8610–8616.

150 L. Lin and Q. Pan, *J. Mater. Chem. A*, 2015, **3**, 1724–1729.

151 P. Xiong, L. Peng, D. Chen, Y. Zhao, X. Wang and G. Yu, *Nano Energy*, 2015, **12**, 816–823.

152 X.-B. Zhong, H.-Y. Wang, Z.-Z. Yang, B. Jin and Q.-C. Jiang, *J. Power Sources*, 2015, **296**, 298–304.

153 J. G. Kim, Y. Kim, Y. Noh and W. B. Kim, *RSC Adv.*, 2014, **4**, 27714–27721.

This journal is © The Royal Society of Chemistry 2016

Energy Environ. Sci., 2016, **9**, 3348–3367 | **3365**

154 D. Bresser, E. Paillard, R. Kloepsch, S. Krueger, M. Fiedler, R. Schmitz, D. Baither, M. Winter and S. Passerini, *Adv. Energy Mater.*, 2013, **3**, 513–523.

155 H. Jia, R. Kloepsch, X. He, M. Evertz, S. Nowak, J. Li, M. Winter and T. Placke, *Acta Chim. Slov.*, 2016, **63**, 470–483.

156 X. Yao, J. Kong, C. Zhao, D. Zhou, R. Zhou and X. Lu, *Electrochim. Acta*, 2014, **146**, 464–471.

157 H. Yue, Q. Wang, Z. Shi, C. Ma, Y. Ding, N. Huo, J. Zhang and S. Yang, *Electrochim. Acta*, 2015, **180**, 622–628.

158 F. Mueller, D. Bresser, E. Paillard, M. Winter and S. Passerini, *J. Power Sources*, 2013, **236**, 87–94.

159 A. Di Cicco, A. Giglia, R. Gunnella, S. L. Koch, F. Mueller, F. Nobili, M. Pasqualini, S. Passerini, R. Tossici and A. Witkowska, *Adv. Energy Mater.*, 2015, **5**, 1500642.

160 L. Cabo-Fernandez, F. Mueller, S. Passerini and L. Hardwick, *Chem. Commun.*, 2016, **52**, 3970–3973.

161 S. J. Rezvani, M. Ciambezi, R. Gunnella, M. Minicucci, M. A. Muñoz-Márquez, F. Nobili, M. Pasqualini, S. Passerini, C. Schreiner, A. Trapananti, A. Witkowska and A. Di Cicco, *J. Phys. Chem. C*, 2016, **120**, 4287–4295.

162 K. Xu, *Chem. Rev.*, 2014, **114**, 11503–11618.

163 C. T. Cherian, M. V. Reddy, G. V. S. Rao, C. H. Sow and B. V. R. Chowdari, *J. Solid State Electrochem.*, 2012, **16**, 1823–1832.

164 X. Tang, X. Hou, L. Yao, S. Hu, X. Liu and L. Xiang, *Mater. Res. Bull.*, 2014, **57**, 127–134.

165 B. Liu, J. Zhang, X. Wang, G. Chen, D. Chen, C. Zhou and G. Shen, *Nano Lett.*, 2012, **12**, 3005–3011.

166 A. Varzi, D. Bresser, J. von Zamory, F. Mueller and S. Passerini, *Adv. Energy Mater.*, 2014, **4**, 1400054.

167 R. van Noorden, *Nature*, 2014, **507**, 26–28.

168 E. J. Berg, C. Villevieille, D. Streich, S. Trabesinger and P. Novák, *J. Electrochem. Soc.*, 2015, **162**, A2468–A2475.

169 K. Naoi, S. Ishimoto, J. Miyamoto and W. Naoi, *Energy Environ. Sci.*, 2012, **5**, 9363–9373.

170 V. Khomenko, E. Raymundo-Piñero and F. Béguin, *J. Power Sources*, 2008, **177**, 643–651.

171 J.-H. Kim, J.-S. Kim, Y.-G. Lim, J.-G. Lee and Y.-J. Kim, *J. Power Sources*, 2011, **196**, 10490–10495.

172 *Standard Potentials in Aqueous Solution*, ed. A. J. Bard, R. Parsons and J. Jordan, Marcel Dekker Inc., New York, U.S.A. & Basel, Switzerland, 1985.

173 R. L. Moss, E. Tzimas, H. Kara, P. Willis and J. Kooroshy, *Energy Policy*, 2013, **55**, 556–564.

174 E. M. Harper, G. Kavlak, L. Burmeister, M. J. Eckelman, S. Erbis, V. Sebastian Espinoza, P. Nuss and T. E. Graedel, *J. Ind. Ecol.*, 2015, **19**, 628–644.

175 P. A. Connor and J. T. Irvine, *Electrochim. Acta*, 2002, **47**, 2885–2892.

176 R. Alcántara, G. F. Ortiz, P. Lavela and J. L. Tirado, *Electrochem. Commun.*, 2006, **8**, 731–736.

177 Y. Qi, N. Du, H. Zhang, P. Wu and D. Yang, *J. Power Sources*, 2011, **196**, 10234–10239.

178 G. Wang, Z. Y. Liu and P. Liu, *Electrochim. Acta*, 2011, **56**, 9515–9519.

179 S. Yuvaraj, S. Amaresh, Y. S. Lee and R. K. Selvan, *RSC Adv.*, 2014, **4**, 6407–6416.

180 C. Chen, Q. Ru, S. Hu, B. An, X. Song and X. Hou, *Electrochim. Acta*, 2015, **151**, 203–213.

181 B. An, Q. Ru, S. Hu, X. Song and C. Chen, *Ionics*, 2015, **21**, 2485–2493.

182 P. A. Connor and J. T. S. Irvine, *J. Power Sources*, 2001, **97–98**, 223–225.

183 C. Hua, X. Fang, Z. Wang and L. Chen, *Chem. – Eur. J.*, 2014, **20**, 5487–5491.

184 S. Lei, K. Tang, C. Chen, Y. Jin and L. Zhou, *Mater. Res. Bull.*, 2009, **44**, 393–397.

185 K. Liang, T. Cheang, T. Wen, X. Xie, X. Zhou, Z. Zhao, C. Shen, N. Jiang and A. Xu, *J. Phys. Chem. C*, 2016, **120**, 3669–3676.

186 F. Huang, Z. Yuan, H. Zhan, Y. Zhou and J. Sun, *Mater. Lett.*, 2003, **57**, 3341–3345.

187 Z. Wang, Z. Wang, W. Liu, W. Xiao and X. W. (David) Lou, *Energy Environ. Sci.*, 2013, **6**, 87–91.

188 G. Fang, S. Kaneko, W. Liu, B. Xia, H. Sun, R. Zhang, J. Zheng and D. Li, *Appl. Surf. Sci.*, 2013, **283**, 963–967.

189 F. Fan, G. Fang, R. Zhang, Y. Xu, J. Zheng and D. Li, *Appl. Surf. Sci.*, 2014, **311**, 484–489.

190 Y. Cao, L. Zhang, D. Tao, D. Huo and K. Su, *Electrochim. Acta*, 2014, **132**, 483–489.

191 X. Li and C. Wang, *RSC Adv.*, 2012, **2**, 6150–6154.

192 L. Fu, K. Song, X. Li, P. A. van Aken, C. Wang, J. Maier and Y. Yu, *RSC Adv.*, 2014, **4**, 36301–36306.

193 I. A. Courtney, W. R. McKinnon and J. R. Dahn, *J. Electrochem. Soc.*, 1999, **146**, 59–68.

194 R. Retoux, T. Brousse and D. M. Schleich, *J. Electrochem. Soc.*, 1999, **146**, 2472–2476.

195 C.-M. Wang, W. Xu, J. Liu, J.-G. Zhang, L. V. Saraf, B. W. Arey, D. Choi, Z.-G. Yang, J. Xiao, S. Thevuthasan and D. R. Baer, *Nano Lett.*, 2011, **11**, 1874–1880.

196 L. Q. Zhang, X. H. Liu, Y.-C. Perng, J. Cho, J. P. Chang, S. X. Mao, Z. Z. Ye and J. Y. Huang, *Micron*, 2012, **43**, 1127–1133.

197 C. J. Pelliccione, Y. Ding, E. V. Timofeeva and C. U. Segre, *J. Electrochem. Soc.*, 2015, **162**, A1935–A1939.

198 Q. Su, Z. Dong, J. Zhang, G. Du and B. Xu, *Nanotechnology*, 2013, **24**, 255705.

199 Y. Zhang, Z. Wang, Y. Li and K. Zhao, *Mech. Mater.*, 2015, **91**, 313–322.

200 L. Liu, F. Xie, J. Lyu, T. Zhao, T. Li and B. G. Choi, *J. Power Sources*, 2016, **321**, 11–35.

201 Z.-W. Fu, F. Huang, Y. Zhang, Y. Chu and Q.-Z. Qin, *J. Electrochem. Soc.*, 2003, **150**, A714–A720.

202 X. Sun, J. Liu and Y. Li, *Chem. Mater.*, 2006, **18**, 3486–3494.

203 R. Demir-Cakan, Y.-S. Hu, M. Antonietti, J. Maier and M.-M. Titirici, *Chem. Mater.*, 2008, **20**, 1227–1229.

204 L. Zhang, H. B. Wu, B. Liu and X. W. (David) Lou, *Energy Environ. Sci.*, 2014, **7**, 1013–1017.

205 J. Liang, X.-Y. Yu, H. Zhou, H. B. Wu, S. Ding and X. W. (David) Lou, *Angew. Chem., Int. Ed.*, 2014, **53**, 12803–12807.

206 Z. Li, J. Ding, H. Wang, K. Cui, T. Stephenson, D. Karpuzov and D. Mitlin, *Nano Energy*, 2015, **15**, 369–378.

207 H. Z. Li, L. Y. Yang, J. Liu, S. T. Li, L. B. Fang, Y. K. Lu, H. R. Yang, S. L. Liu and M. Lei, *J. Power Sources*, 2016, **324**, 780–787.

3366 | *Energy Environ. Sci.*, 2016, **9**, 3348–3367

This journal is © The Royal Society of Chemistry 2016

208 J. Ding, Z. Li, H. Wang, K. Cui, A. Kohandehghan, X. Tan, D. Karpuzov and D. Mitlin, *J. Mater. Chem. A*, 2015, **3**, 7100–7111.

209 P. Meduri, C. Pendyala, V. Kumar, G. U. Sumanasekera and M. K. Sunkara, *Nano Lett.*, 2009, **9**, 612–616.

210 G.-L. Xu, Y. Li, T. Ma, Y. Ren, H.-H. Wang, L. Wang, J. Wen, D. Miller, K. Amine and Z. Chen, *Nano Energy*, 2015, **18**, 253–264.

211 S. Böhme, K. Edström and L. Nyholm, *Electrochim. Acta*, 2015, **179**, 482–494.

212 L. Q. Zhang, X. H. Liu, Y. Liu, S. Huang, T. Zhu, L. Gui, S. X. Mao, Z. Z. Ye, C. M. Wang, J. P. Sullivan and J. Y. Huang, *ACS Nano*, 2011, **5**, 4800–4809.

213 B. Oschmann, M. N. Tahir, F. Mueller, D. Bresser, I. Lieberwirth, W. Tremel, S. Passerini and R. Zentel, *Macromol. Rapid Commun.*, 2015, **36**, 1075–1082.

214 O. B. Chae, S. Park, J. H. Ryu and S. M. Oh, *J. Electrochem. Soc.*, 2013, **160**, A11–A14.

215 L. MacEachern, R. A. Dunlap and M. N. Obrovac, *J. Electrochem. Soc.*, 2015, **162**, A229–A234.

216 J. S. Chen, C. M. Li, W. W. Zhou, Q. Y. Yan, L. A. Archer and X. W. Lou, *Nanoscale*, 2009, **1**, 280–285.

217 J. Morales and L. Sánchez, *J. Electrochem. Soc.*, 1999, **146**, 1640–1642.

218 Y. Zhong, M. Yang, X. Zhou and Z. Zhou, *Mater. Horiz.*, 2015, **2**, 553–566.

219 Y. Yang, Q. Liang, J. Li, Y. Zhuang, Y. He, B. Bai and X. Wang, *Nano Res.*, 2011, **4**, 882–890.

220 C. Tang, J. Sheng, C. Xu, S. M. B. Khajehbashi, X. Wang, P. Hu, X. Wei, Q. Wei, L. Zhou and L. Mai, *J. Mater. Chem. A*, 2015, **3**, 19427–19432.

221 S.-H. Yu, B. Quan, A. Jin, K.-S. Lee, S. H. Kang, K. Kang, Y. Piao and Y.-E. Sung, *ACS Appl. Mater. Interfaces*, 2015, **7**, 25725–25732.

222 Y.-Y. Wang, T. Li, Y.-X. Qi, R.-L. Bai, L.-W. Yin, H. Li, N. Lun and Y.-J. Bai, *Electrochim. Acta*, 2015, **186**, 572–578.

223 F. Zhang, Y. An, W. Zhai, X. Gao, J. Feng, L. Ci and S. Xiong, *Mater. Res. Bull.*, 2015, **70**, 573–578.

224 Q. Zhang, S. Ge, H. Xue, X. Wang, H. Sun and A. Li, *RSC Adv.*, 2014, **4**, 58260–58264.

225 X. Wei, C. Tang, X. Wang, L. Zhou, Q. Wei, M. Yan, J. Sheng, P. Hu, B. Wang and L. Mai, *ACS Appl. Mater. Interfaces*, 2015, **7**, 26572–26578.

226 F. Mueller, D. Bresser, N. Minderjahn, J. Kalhoff, S. Menne, S. Krueger, M. Winter and S. Passerini, *Dalton Trans.*, 2014, **43**, 15013–15021.

227 W. Cheng, F. Rechberger, G. Ilari, H. Ma, W.-I. Lin and M. Niederberger, *Chem. Sci.*, 2015, **6**, 6908–6915.

228 I. D. Raistrick, C. Ho and R. A. Huggins, *J. Electrochem. Soc.*, 1976, **123**, 1469–1476.

229 B. Guo, J. Shu, Z. Wang, H. Yang, L. Shi, Y. Liu and L. Chen, *Electrochem. Commun.*, 2008, **10**, 1876–1878.

230 A. Veluchamy, C.-H. Doh, D.-H. Kim, J.-H. Lee, D.-J. Lee, K.-H. Ha, H.-M. Shin, B.-S. Jin, H.-S. Kim, S.-I. Moon and C.-W. Park, *J. Power Sources*, 2009, **188**, 574–577.

231 A. D. W. Todd, R. E. Mar and J. R. Dahn, *J. Electrochem. Soc.*, 2006, **153**, A1998–A2005.

232 J. R. Dahn, R. E. Mar and A. Abouzeid, *J. Electrochem. Soc.*, 2006, **153**, A361–A365.

233 A. D. W. Todd, R. E. Mar and J. R. Dahn, *J. Electrochem. Soc.*, 2007, **154**, A597–A604.

234 Q. Fan, P. J. Chupas and M. S. Whittingham, *Electrochem. Solid-State Lett.*, 2007, **10**, A274–A278.

235 O. Mao, R. A. Dunlap and J. R. Dahn, *J. Electrochem. Soc.*, 1999, **146**, 405–413.

236 R. Nagai, F. Kita, M. Yamada and H. Katayama, *Hitachi Rev.*, 2011, **60**, 28–32.

237 M. Miyachi, H. Yamamoto and H. Kawai, *J. Electrochem. Soc.*, 2007, **154**, A376–A380.

238 P. Heitjans and S. Indris, *J. Phys.: Condens. Matter*, 2003, **15**, R1257–R1289.

239 M. M. Islam and T. Bredow, *J. Phys. Chem. C*, 2009, **113**, 672–676.

240 Y. Nishi, *Chem. Rec.*, 2001, **1**, 406–413.

241 X. H. Liu, S. Huang, S. T. Picraux, J. Li, T. Zhu and J. Y. Huang, *Nano Lett.*, 2011, **11**, 3991–3997.

242 J. Graetz, C. C. Ahn, R. Yazami and B. Fultz, *J. Electrochem. Soc.*, 2004, **151**, A698–A702.

243 H. Jia, R. Kloepsch, X. He, J. P. Badillo, P. Gao, O. Fromm, T. Placke and M. Winter, *Chem. Mater.*, 2014, **26**, 5683–5688.

244 X.-L. Wang, W.-Q. Han, H. Chen, J. Bai, T. A. Tyson, X.-Q. Yu, X.-J. Wang and X.-Q. Yang, *J. Am. Chem. Soc.*, 2011, **133**, 20692–20695.

245 U. v. Alpen, A. Rabenau and G. H. Talat, *Appl. Phys. Lett.*, 1977, **30**, 621–623.

246 G. Nazri, *MRS Proc.*, 1988, **135**, 117.

247 D. H. Gregory, *Chem. Rec.*, 2008, **8**, 229–239.

248 W. Li, G. Wu, C. M. Araujo, R. H. Scheicher, A. Blomqvist, R. Ahuja, Z. Xiong, Y. Feng and P. Chen, *Energy Environ. Sci.*, 2010, **3**, 1524–1530.

249 P. F. Teh, S. S. Pramana, C. Kim, C.-M. Chen, C.-H. Chuang, Y. Sharma, J. Cabana and S. Madhavi, *J. Phys. Chem. C*, 2013, **117**, 24213–24223.

This journal is © The Royal Society of Chemistry 2016

Energy Environ. Sci., 2016, **9**, 3348–3367 | 3367